Macromolecules

Article

Cite This: Macromolecules 2019, 52, 4858−4874

pubs.acs.org/Macromolecules

Bridging Simulation Length Scales of Bottlebrush Polymers Using a Wormlike Cylinder Model

Sarit Dutta,[†] Tianyuan Pan,[‡] and Charles E. Sing*,[†]

[†]Department of Chemical and Biomolecular Engineering and [‡]Department of Materials Science and Engineering, University of Illinois at Urbana-Champaign, Urbana, Illinois 61801, United States

Supporting Information

ABSTRACT: Bottlebrush polymers, formed from a linear backbone polymer with a high density of grafted side chains, are functional macromolecules useful in molecular assembly and responsive materials due to their unique physical properties. Interactions between the side chains stiffen the molecular backbone and imbue it with a molecular dimension beyond simply the polymer length, drastically altering dynamic relaxation and intrapolymer interactions. Simulation prediction of these material properties remains a challenge, however, because they specifically depend on side chain degrees of freedom that are computationally expensive to model. In this work, we use the wormlike cylinder framework to systematically map molecular features from a single-molecule hybrid Brownian dynamics and Monte Carlo (BD/MC) simulation with explicit side chains to a simple touched-bead polymer model. We use static properties from the explicit side chain simulations such as end-to-end distance and radius of gyration to parameterize the wormlike cylinder model and consistently reproduce other single-chain properties such as hydrodynamic radius and intrinsic viscosity. This parameterization yields the stiffness parameter and equivalent diameter of a bottlebrush and is compared to prior scaling theories and simulation results. We find that the wormlike cylinder model, appropriately parameterized, provides an accurate description of these quantities over a wide range of side chain lengths and grafting densities. We demonstrate that a coarse-grained representation is able to consistently reproduce the bottlebrush structure and show that the wormlike cylinder model can be useful for large-scale coarse-grained simulations of bottlebrush suspensions.

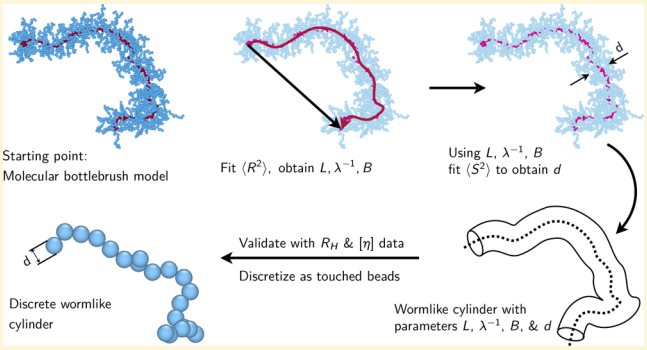

1. INTRODUCTION

Over the past two decades densely grafted polymers, called "bottlebrushes", have emerged as an exciting subclass of branched macromolecules. Bottlebrush polymers have found utility as building blocks for a wide range of novel materials,[1] for example, photonic[2−4] and phononic crytals,[5] molecular pressure sensors,[6,7] pressure sensitive adhesives,[8] pH-responsive surfaces,[9] stimuli-responsive molecular brushes,[10] and low-modulus elastomers capable of strain hardening and sustaining large deformation.[11−15] These applications make use of the unique properties of bottlebrush polymers, which emerge from the more extended conformations bottlebrushes exhibit compared to linear chains of the same length, and the considerable stiffening of the backbone or even the side chains at high grafting densities. The stiffening of the backbone causes reduced molecular entanglements in bottlebrush melts,[16−18] and in suspensions, lyotropic ordering has been reported.[19−21] These recent efforts to use bottlebrush polymers in functional and self-assembly applications point to the need to study a large-scale macroscopic behavior (e.g., rheology or self-assembly) of bottlebrush suspensions and melts and understand how to tune these properties using an expanded list of molecular architecture parameters (e.g., side chain length and density and backbone length).

To address this need, a large variety of molecular models have been used to predict or explain the behavior of bottlebrush polymers. This is particularly prevalent in the simulation literature, with a wide range of simulation models to try to capture the conformational properties of bottlebrush polymers. Efforts include Monte Carlo (MC) simulations (both lattice-based[22] and off-lattice[23−33]), bond fluctuation models,[34−36] cellular automaton models,[37] molecular dynamics (MD) models,[15,38−51] and Brownian dynamics (BD) models.[52] In addition, numerical theory such as self-consistent field theory[53,54] and polymer reference interaction site model (PRISM) theory[55] have also been used to capture the conformational attributes of bottlebrush polymers. The focus of most of these studies is to understand the key questions of bottlebrush conformation, namely, how do densely grafted side chains stiffen the backbone, and how do we quantify the

Received: February 19, 2019
Revised: May 30, 2019
Published: June 18, 2019

DOI: 10.1021/acs.macromol.9b00363
Macromolecules 2019, 52, 4858−4874

stiffness of the bottlebrush via a Kuhn length or persistence length? This is crucial for understanding the origin of a bottlebrush structure, particularly the size (e.g., end-to-end distance, radius of gyration, and hydrodynamic radius) and shape (e.g., asphericity and prolateness). The predominant approach in these studies has been to characterize the scaling exponents of these size measures as a function of backbone or side chain degree of polymerization and in turn contextualize the molecular stiffness. This has been complementary to scaling theories that extend the theoretical knowledge of chain statistics to bottlebrush architectures, which similarly provide predictions of scaling exponents.[34,56−59] Despite the significant success in modeling bottlebrush conformation, there remain significant computational limitations on the time scale and length scale over which these molecules can be simulated. This is especially limiting for large bottlebrushes, which can have ∼100−1000 side chains, where simulations are essentially limited to a single bottlebrush. The large-scale rheological and self-assembly properties that are sought after in bottlebrushes are thus challenging to predict, especially with molecular simulation.

The most costly aspect of the simulation and theory of the bottlebrush polymer structure is the need to resolve the side chain degrees of freedom. This is crucial, because the observed stiffness is not intrinsic to the backbone but related to the architecture and interactions between the side chains. Indeed, it is describing this side chain-induced stiffness that is often the main motivation of the both simulation and theory. However, experimental investigations often take a different approach that does not rely on the resolution of side chains. Here, the experimental literature describes bottlebrush polymers as a wormlike cylinder (WLCy), which was considered in a series of early papers by Wintermantel and co-workers.[20,60,61] Initial studies demonstrated that the WLCy model matched well to the radius of gyration and hydrodynamic radius,[20,60−64] and later work extended the original WLCy model to show that the static structure factor, center-of-mass diffusivity, and intrinsic viscosity can all be consistently described by taking chain ends into consideration.[65−70] While much of this work focuses on flexible side chains, the model can also be used to describe bottlebrushes with semiflexible or rodlike side chains.[3,71−75] Much of this literature has been reviewed extensively by Nakamura and Norisuye.[76]

There are thus two different general approaches to studying bottlebrushes: in the simulation and theory approach, conformational features (e.g., radius of gyration, end-to-end distance) emerge naturally out of explicitly modeled side chains; in experimental efforts that use the WLCy model, the same conformational features serve as a route to parameterize and validate predictions that emerge from an assumed molecular geometry without any input regarding its architectural origin. While ostensibly describing the same molecular conformations, seemingly conflicting observations emerge. For example, simulation and scaling theory generally agrees that scaling exponents are similar to that of a flexible chain for synthetically relevant cases.[28,49,56] This is curiously distinct from the results that the Kuhn length of a bottlebrush can be as much as 40−100 times larger than that of a flexible backbone, as measured in an experiment assuming a wormlike geometry.[61,77−80] In contrast to a flexible chain, this suggests that bottlebrushes possess significant rigidity, consistent with experimental evidence of lyotropic ordering of bottlebrushes in nondilute solutions.[19−21] This prediction is also consistent with some simulation[49] and theory[57] for the bottlebrush persistence length.

In this paper, we explore the possibility of using the WLCy model as a coarse-grained representation of a bottlebrush in a way that parameterizes the molecular simulation rather than the experimental observation. The latter molecular model is based on a hybrid BD/MC simulation model developed by the authors, with properties that arise from resolving the side chain structure and in quantitative agreement with the experiment.[52] We focus on four quantities— end-to-end distance $\langle R^2 \rangle$, radius of gyration $\langle S^2 \rangle$, hydrodynamic radius R_H, and intrinsic viscosity $[\eta]$—to show that the wormlike cylinder model can accurately capture the results of the underlying fine-grained model. We use a parameterization procedure that systematically shows that the WLCy model is consistent among a wide range of conformational and dynamic properties and for a large number of polymer architectures (e.g., side chain length, backbone length, and grafting density). The parameters of the WLCy model provide insight into a wide range of conformational features such as the molecular width and flexibility, and we demonstrate how the scaling exponent for the flexible chain arises from a relatively stiff molecule. We also show that, by parameterizing the WLCy model from a computationally expensive molecular simulation with explicit side chains, we can develop a coarse-grained model of a bottlebrush that has implicit side chains. This model is currently focused on dilute suspensions of bottlebrush polymers, with nondilute systems requiring additional study of inter-bottlebrush interactions. However, this implicit side chain representation represents the first step to carrying out large-scale simulations of bottlebrush suspensions, which would otherwise be computationally intractable in more fine-grained polymer simulations.

2. BOTTLEBRUSH MODEL AND SIMULATION METHOD

We use a simulation model of bottlebrush polymers developed in our prior work,[52] which includes explicit side chains and can be quantitatively compared to the experimental results for intrinsic viscosity and hydrodynamic radius.[52] This model represents the bottlebrush architecture via a coarse-grained bead-spring model, with the backbone consisting of N_{bb} beads and each side chain consisting of N_{sc} beads. The grafting density, f, determines the number of side chains attached to a backbone bead. For example, if $f = 2$, then two side chains are connected to each backbone bead, whereas $f = 0.5$ indicates one side chain every two backbone beads. It is possible to map the parameters N_{sc} and N_{bb} to synthetic bottlebrush degrees of polymerization, specifically for poly(lactic acid) side chains grafted to a poly(norbornene) backbone, for the special case that $f = 1$.[52]

This bottlebrush model considers an overall energy, $U = U_s + U_{ev} + U_b$, that includes a spring potential U_s, an excluded volume potential U_{ev}, and a bending potential U_b. For the spring potential, we use finitely extensible nonlinear elastic (FENE) springs to maintain the connectivity between the beads:

$$U_s = -\sum_{i,j} * \frac{1}{2} k_s r_{max}^2 \log\left[1 - \left(\frac{r_{ij}}{r_{max}}\right)^2\right], \quad r_{ij} < r_{max} \tag{1}$$

Here, the spring constant is $k_s = 30\varepsilon/\sigma^2$ and the maximum spring extension is $r_{max} = 1.5\sigma$, where r_{ij} is the distance between

DOI: 10.1021/acs.macromol.9b00363
Macromolecules 2019, 52, 4858−4874

the two connecting beads, and σ and ε are the length and energy parameters (in unit of k_BT, where k_B is the Boltzmann constant and T is the absolute temperature), respectively.[81] The summation is marked by an asterisk to indicate that it is over the connected bead pairs, as determined by the bottlebrush topology.

The Weeks−Chandler−Anderson (WCA) potential[82] is used to model the pairwise excluded volume between the beads:

$$U_{ev} = \sum_{i,j>i}^{*} \begin{cases} 4\varepsilon\left[\left(\frac{\sigma}{r_{ij}}\right)^{12} - \left(\frac{\sigma}{r_{ij}}\right)^{6}\right] & r_{ij} < r_c \\ -4\varepsilon\left[\left(\frac{\sigma}{r_c}\right)^{12} - \left(\frac{\sigma}{r_c}\right)^{6}\right], & \\ 0, & \text{otherwise} \end{cases} \quad (2)$$

where $r_c = 2^{1/6}\sigma$. This form of U_{ev} models a bottlebrush under athermal conditions. Finally, a bending potential is given as

$$U_b = \sum_{i,j}^{*} \frac{1}{2} k_B T(1 - \cos\theta_{ij}) \quad (3)$$

This potential is introduced only for beads constituting the backbone, where $\theta_{ij} = \cos^{-1}(\hat{\mathbf{u}}_j \cdot \hat{\mathbf{u}}_i)$ is the bond angle (complementary) between the unit vectors $\hat{\mathbf{u}}_j$ and $\hat{\mathbf{u}}_i$ along consecutive backbone bonds.

The beads are assigned a hydrodynamic radius a and a drag coefficient ζ, representing the friction of a bead. Assuming $a = \sigma/2$ and $\zeta = 6\pi\eta_s a$, where η_s is the solvent viscosity, the bead diffusivity is k_BT/ζ, and the bead diffusion time is $\tau = \zeta a^2/kT$. We choose a as the unit of length, k_BT as the unit of energy, and τ as the unit of time. Consequently, the unit of force is k_BT/a, and the unit of diffusivity is k_BT/ζ.

We use a combination of Brownian dynamics[83] (BD) and Monte Carlo (MC) to evolve the bead positions. The BD position update is via the discretized stochastic differential equation

$$\mathbf{R}(t + \delta t) = \mathbf{R}(t) - \mathbf{D}(t)\cdot\nabla U(t)\delta t + \sqrt{2\delta t}\ \mathbf{D}^{1/2}\cdot\mathbf{x} \quad (4)$$

where $\mathbf{R}$ is the column vector of all bead positions, $\mathbf{D}$ is the $3N \times 3N$ diffusivity tensor (N being the total number of beads), δt is the time step, and $\mathbf{x}$ is a column vector of length $3N$ containing random numbers drawn from a normal distribution $N(0,1)$. The third term $\sqrt{2\delta t}\ \mathbf{D}^{1/2}\cdot\mathbf{x}$ represents the displacement only due to Brownian motion. The right-hand side of the above equation is evaluated using the positions at time t and left-hand side gives the bead positions at time $t + \delta t$. Note that eq 4 is in a nondimensionalized form with respect to the units mentioned in the preceding paragraph. Furthermore, for computational expediency, we neglect the hydrodynamic interaction (HI) between the beads; therefore, the diffusivity tensor $\mathbf{D}$ degenerates to an identity matrix.

Two kinds of MC moves—(i) backbone pivot and (ii) side chain double bridging—are used periodically after several BD steps to induce rapid global conformational changes as described in ref 52. Six independent trajectories were generated for each case. The time step δt for advancing the beads was $10^{-4}\tau$. A pivot move was performed after every 50 BD time steps, and a double bridging sweep was performed after every 11 BD time steps. A sweep involves performing the double-bridging move described earlier repeatedly so as to cover approximately half of the total number of beads. The total duration of all trajectories was 10^8 time steps or more. We checked the approach to equilibrium by monitoring global size measures of the whole bottlebrush ($\langle S^2\rangle$ and R_H) and that of the backbone and side chains separately. Properties calculated subsequently were averaged over all the trajectories. Errors analysis was performed using by the block-averaging procedure.

The diffusion coefficient was calculated from the so-called Kirkwood diffusivity:[84]

$$D^K = \frac{1}{3N^2}\sum_i\sum_j \mathrm{Tr}\langle\mathbf{D}_{ij}\rangle \quad (5)$$

where $\mathbf{D}_{ij}$ is the Rotne−Prager−Yamakawa (RPY) tensor,[85,86] which accounts for the hydrodynamic interaction between bead i and bead j, N is the total number of beads, and the angle brackets denote average over all conformations. The hydrodynamic radius R_H is then determined using the Stokes−Einstein relation

$$R_H = \frac{k_BT}{6\pi\eta_s D^K} \quad (6)$$

where η_s is the solvent viscosity. In eq 5, the 3×3 blocks $\mathbf{D}_{ij}$ of the diffusivity tensor are given by

$$\mathbf{D}_{ij} = (1 - \delta_{ij})\mathbf{\Omega}_{ij} + \delta_{ij}\mathbf{I}, \quad i, j = 1, ..., N \quad (7)$$

where δ_{ij} is the Kronecker delta, $\mathbf{I}$ is the 3×3 identity matrix, and

$$\mathbf{\Omega}_{ij} = \begin{cases} \frac{3a}{4r_{ij}}\left[\left(1 + \frac{2a^2}{3r_{ij}^2}\right)\mathbf{I} + \left(1 - \frac{2a^2}{r_{ij}^2}\right)\frac{\mathbf{r}_{ij}\mathbf{r}_{ij}}{r_{ij}^2}\right], & r_{ij} \geq 2a \\ \left(1 - \frac{9r_{ij}}{32a}\right)\mathbf{I} + \left(\frac{3r_{ij}}{32a}\right)\frac{\mathbf{r}_{ij}\mathbf{r}_{ij}}{r_{ij}^2}, & r_{ij} < 2a \end{cases} \quad (8)$$

The averaging in eq 5 was performed on equilibrium conformations obtained from a simulation run.

We calculate the intrinsic viscosity $[\eta]$ using the expression[87−90]

$$\frac{[\eta]M}{\pi N_A a^3} = \left(\frac{10}{3}\right)N + \frac{1}{a^2}\left\langle \frac{\sum_i R_i^2}{1 + \left(\frac{3a}{4}\right)\frac{Q}{\sum_i R_i^2}} \right\rangle \quad (9)$$

where N_A is the Avogadro's number, N is the total number of beads, M is the molecular weight, and

$$Q = \sum_l\sum_s{}' \left[\frac{\mathbf{R}_l\cdot\mathbf{R}_s}{R_{ls}} + \frac{1}{10R_{ls}^3}\{4(R_l^2 + R_s^2)\mathbf{R}_l\cdot\mathbf{R}_s - R_l^2R_s^2 - 7(\mathbf{R}_l\cdot\mathbf{R}_s)^2\}\right]$$

where $\mathbf{R}_i$ is the position vector of bead i with respect to the molecule center-of-mass, $R_i = \|\mathbf{R}_i\|$, and $R_{ij} = \|\mathbf{R}_i - \mathbf{R}_j\|$.

In eq 9, the first term in the left-hand side is a correction term introduced to account for the limiting case of a single bead,[87] the expression inside the angle brackets was derived by Tsuda[89] for rigid molecules based a nonpreaveraged version of

DOI: 10.1021/acs.macromol.9b00363
Macromolecules 2019, 52, 4858−4874

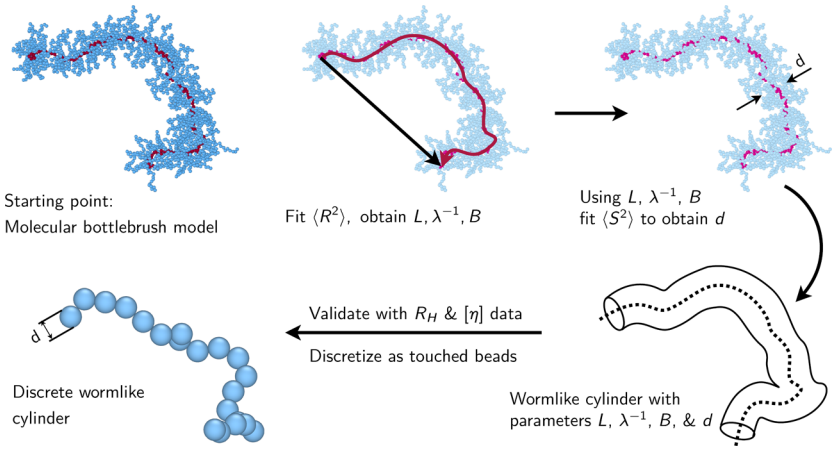

Figure 1. Schematic showing the extraction of model parameters from the bottlebrush simulation data. Fine-grained models using explicit side chains are first systematically parameterized by fitting $\langle R^2 \rangle$ using the length L, Kuhn length λ^{-1}, and excluded volume parameter B. Subsequently, the diameter d is determined from fitting the radius of gyration $\langle S^2 \rangle$. This sets all the parameters for the wormlike cylinder model, which can then be validated with predictions for hydrodynamic radius R_H and intrinsic viscosity $[\eta]$. Once we have a consistent set of WLCy parameters, we can use these to represent a bottlebrush with an implicit side chain model based on a discrete wormlike cylinder.

Kirkwood theory, and the angle brackets were put in by de la Torre et al.[88] to account for conformational fluctuations in flexible molecules. The average denoted by the angle brackets in eq 23 was performed on the conformations obtained from simulations.

3. PARAMETERIZATION OF THE WLCY MODEL

3.1. Parameterization Overview. The WLCy model is a Kratky−Porod (KP) chain with a finite diameter and uses three molecular parameters: contour length L, Kuhn length λ^{-1}, cylinder diameter d.[91−93] In this work, we occasionally also include an excluded volume parameter B that accounts for situations where the cylinder interacts with itself significantly (i.e., in the limit of a flexible and/or long bottlebrushes). This enters the formalism via the quasi-two parameter (QTP) theory,[92] which perturbatively considers the effect of excluded volume on the observables we measure. We show that this model is capable of capturing the behaviors observed in our molecular BD/MC simulations but implement a systematic protocol for determining these four parameters.

The general scheme we used is shown in Figure 1. The bottlebrush end-to-end distance is first used to determine values of L, λ^{-1}, and B, representing a smaller subset of the molecular parameters of interest. B is only incorporated as needed. The value of d does not play a role in the end-to-end distance but does factor into the WLCy prediction of the mean-square radius of gyration $\langle S^2 \rangle$; we fit using the previously determined values of L, λ^{-1}, and B to determine d. With the four parameters determined, we can then test this prediction against the hydrodynamic radius R_H, intrinsic viscosity $[\eta]$, and form factor $P(qa)$. This may not be the only route to parameterizing the WLCy model to our data but is the most straightforward due to the simplicity of using the end-to-end distance to obtain the initial parameters. Other routes to parameterization, such as initially fitting other values like R_H before the end-to-end distance, are significantly more numerically challenging; as such, we demonstrate the suitability of the parameters obtained by this procedure by appealing to their success in describing the bottlebrush properties. Indeed, we will ultimately show that the WLCy parameters are consistent across all of the aforementioned observables, suggesting that this straightforward model is an excellent minimal model of a bottlebrush polymer.

3.2. End-to-End Distance Parameterization. We begin by using the mean-square end-to-end distance $\langle R^2 \rangle$ to parameterize L, λ^{-1}, and B. In experimental studies, L is typically not known a priori but rather assumed to be proportional to the molecular weight M. In the case of simulation, we introduce a constant of proportionality $m_L = L/(N_{bb} - 1)$ as a fitting parameter, which parameterizes the connection between the number of simulation backbone beads N_{bb} and the effective length of the chain.

We fit using an expression for $\langle R^2 \rangle$, which, in the absence of excluded volume effects, is given by the standard expression for a KP chain:[91]

$$\langle R^2 \rangle_0 = \frac{L}{\lambda} - \frac{1}{2\lambda^2}(1 - e^{-2\lambda L}) \tag{10}$$

This equation only requires two parameters (L and λ^{-1}), with the diameter d and excluded volume parameter B not appearing. In the case that the chain is sufficiently long and flexible, it will be important to include excluded volume via the QTP theory.[92] The quantity $B \geq 0$ serves as a measure of the excluded volume strength, with dimensions of length, and is related to the binary cluster integral (ref 94, pp. 61) $\beta = 4\pi\int_0^\infty [1 - \exp(-u(r)/k_BT)]\, r^2 dr$ via $B = \beta/a^2$, where a is the spacing between the beads along the contour and $u(r)$ is the potential of mean force between the two beads. In the QTP formalism[92]

$$\langle R^2 \rangle = \alpha_R^2 \langle R^2 \rangle_0 \tag{11}$$

where

$$\alpha_R^2 = \left[1 + 10\tilde{z} + \left(\frac{70\pi}{9} + \frac{10}{3}\right)\tilde{z}^2 + 8\pi^{3/2}\tilde{z}^3\right]^{2/15} \tag{12}$$

Here, the quantity $\tilde{z}$ is given as

$$\tilde{z} = 0.75K\left(\frac{3}{2\pi}\right)^{3/2} \lambda B(\lambda L)^{1/2} \tag{13}$$

where

DOI: 10.1021/acs.macromol.9b00363
Macromolecules 2019, 52, 4858−4874

$$K = \begin{cases} \frac{4}{3} - \frac{2.711}{(\lambda L)^{1/2}} + \frac{7}{6\lambda L}, & \lambda L > 6 \\ \exp[0.9198 - 6.611(\lambda L)^{-1} + 0.03516\lambda L](\lambda L)^{-1/2}, & \lambda L \leq 6 \end{cases}$$

The resulting fits are tabulated in Tables 1−4. For $f = 1$, beyond $N_{sc} = 8$, we find that simple two-parameter fits with m_L and λ^{-1} are sufficient to describe the simulation data. Indeed, the excluded volume parameter appears as an extraneous parameter in these cases and cannot be determined reliably. We interpret these cases as the contour length L being short enough so as to fall outside the excluded volume regime. Note that the excluded volume referred to here is the long-range interaction along the backbone of the WLCy, not the excluded volume inherent in a bead-spring model. For $f = 2$, we find that determination of B is not required beyond $N_{sc} = 4$; for $f = 5$, none of the values of N_{sc} treated here requires consideration of excluded volume (B and λB are not listed in Table 4). We also note that that value of B has units of length and is due to the steric repulsion between the densely packed side chains; however, B is not the same as the molecular width, d, which is a geometric measure of the chain conformation. In our model, we treat these quantities as independent parameters, as we are unaware of any known relationship between these two quantities in the context of bottlebrush polymers. Figure 2 shows the simulation data along with fits to the WLCy model for cases both including and excluding B. Satisfyingly, a single set of values m_L, λ^{-1}, and B can fit the entire curves for $\langle R^2 \rangle$ as a function of N_{bb} for all simulation measurements spanning different values of f and N_{sc}.

Table 1. Fitting Parameters for $f = 0.5$

N_{sc}	m_L	λ^{-1}	d	B	λd	λB
2	1.385	10.861	4.932	6.298	0.454	0.580
4	1.277	14.739	7.623	12.972	0.517	0.880
8	1.088	28.841	12.214	29.365	0.423	1.018
14	1.011	50.855	17.286	56.394	0.340	1.109
20	0.974	80.048	21.665	71.987	0.271	0.899
32	0.967	125.28	28.708	149.72	0.229	1.195

Table 2. Fitting Parameters for $f = 1$

N_{sc}	m_L	λ^{-1}	d	B	λd	λB
2	1.342	16.003	5.461	9.822	0.341	0.614
4	1.244	28.115	8.138	18.137	0.289	0.645
8	1.179	57.879	12.538	29.364	0.217	0.507
14	1.143	119.168	18.048		0.151	
20	1.133	182.40	22.755		0.099	
32	1.121	351.84	30.590		0.087	

Table 3. Fitting Parameters for $f = 2$

N_{sc}	m_L	λ^{-1}	d	B	λd	λB
2	1.466	23.547	5.759	11.164	0.245	0.474
4	1.424	48.332	8.503	11.826	0.176	0.245
8	1.416	111.57	13.210		0.118	
14	1.404	253.96	19.295		0.076	
20	1.405	736.49	24.337		0.033	

Table 4. Fitting Parameters for $f = 5$

N_{sc}	m_L	λ^{-1}	d	λd
2	1.955	52.837	5.612	0.106
4	1.975	116.76	8.546	0.073
8	1.990	306.52	13.841	0.046
14	2.007	603.13	20.603	0.034
20	1.977	1541.0	27.006	0.017

3.3. Radius of Gyration Parameterization. Having obtained m_L, λ^{-1}, and B (where applicable), we now fit only for d based on the radius of gyration from the same set of molecular simulations used to plot $\langle R^2 \rangle$ in Figure 2. The mean-square radius of gyration $\langle S \rangle_0$ for an unperturbed WLCy is[93]

$$\langle S^2 \rangle_0 = \frac{L}{6\lambda} - \frac{1}{4\lambda^2} + \frac{1}{4\lambda^3 L} - \frac{1}{8\lambda^4 L^2}(1 - e^{-2\lambda L}) + \frac{d^2}{8} \quad (14)$$

Here, the value of d only enters in as a correction to account for the effect of chain ends, which we assume to be hemispheric with a diameter equivalent to d. Nevertheless, because we have already obtained the other parameters, we can calculate d to reasonable accuracy. We also use a QTP expression for long, flexible chains where B was necessary to fit $\langle R^2 \rangle$, but now for

$$\langle S^2 \rangle = \alpha_S^2 \langle S^2 \rangle_0 \quad (15)$$

where

$$\alpha_S^2 = [0.933 + 0.067 \exp(-0.85\tilde{z} - 1.39\tilde{z}^2)]\alpha_R^2 \quad (16)$$

This correction is only dependent on $\tilde{z}$ and thus L and B, so it has already been set in the previous step of the parameterization protocol. We show the importance of this correction in the Supporting Information by plotting KP/QTP predictions against the simulation data with and without the excluded volume effect, B. With the KP and QTP expressions combined, we show the corresponding fits in Figure 3 and the fit values tabulated in Tables 1−4. We note that, in Figure 3, we distinguish between the values of $\langle S^2 \rangle$ of just the backbone beads (solid points) and the value of $\langle S^2 \rangle$ for the entire bottlebrush (open points). This highlights the role of d, which leads to the deviations at low N_{bb}. It is this limit where d becomes the major contributor in eq 15, and we once again note that we can fit the WLCy model to the simulation data almost exactly. This completes our parameterization of the entire set of bottlebrush simulations, which can now be tested against other conformational observables.

3.4. Consistency of the WLCy Model with Hydrodynamic Radius and Intrinsic Viscosity. The WLCy model can be used to predict hydrodynamic radius R_H, and a related touched-bead model can be used to predict the intrinsic viscosity $[\eta]$. These provide a consistency check so that it is possible to determine how well the WLCy parameters m_L, λ^{-1}, B, and d reproduce simulation observations that are not directly related to the values $\langle R^2 \rangle$ and $\langle S^2 \rangle$.

We first calculate the hydrodynamic radius $R_{H,0}$ for an unperturbed WLCy when $L > 4d$:[95]

DOI: 10.1021/acs.macromol.9b00363
Macromolecules 2019, 52, 4858−4874

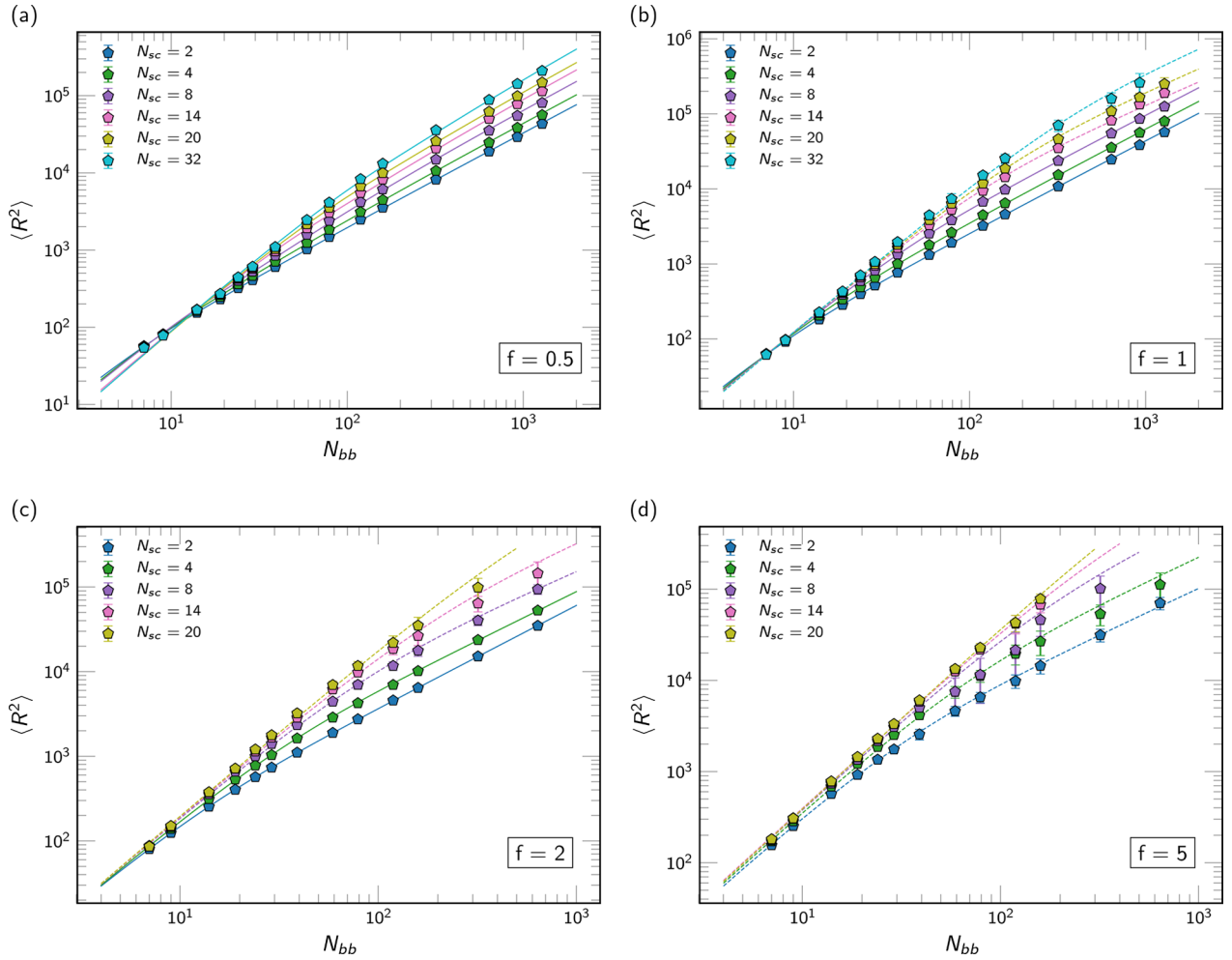

Figure 2. Mean-square end-to-end distance $\langle R^2 \rangle$ as a function of backbone DP N_{bb} for different grafting densities: (a) $f = 0.5$, (b) $f = 1$, (c) $f = 2$, and (d) $f = 5$. Markers denote the simulation data, solid lines denote fits considering the excluded volume interaction (eq 11), and dashed lines denote fits neglecting the effect of excluded volume (eq 10). Fit parameters m_L, λ^{-1}, and B are tabulated in Tables 1−4 for all values of N_{sc} and f.

$$\frac{1}{R_{H,0}} = \begin{cases} \frac{2}{L}[C_0 \ln \sigma + C_1 + C_2\lambda L + C_3(\lambda L)^2 + C_4(\lambda L)^3 + C_5\sigma^{-1} \ln \sigma + C_6\sigma^{-1} + C_7\sigma^{-2} + C_8\sigma^{-3} + C_9\sigma^{-4}], & \lambda L \leq 2.278 \\ \frac{2}{L}[A_0(\lambda L)^{1/2} + A_1A_2(\lambda L)^{-1/2} + A_3(\lambda L)^{-1} + A_4(\lambda L)^{-3/2}], & \lambda L > 2.278 \end{cases} \quad (17)$$

where $\sigma = L/d$. The coefficients A_i and C_j are given in ref 95. In this limit ($L \geq 4d$), we can (when necessary) use the QTP theory prediction

$$R_H = \alpha_H R_{H,0} \quad (18)$$

where

$$\alpha_H = (1 + 6.02\tilde{z} + 3.59\tilde{z}^2)^{1/10} \quad (19)$$

For $L \leq 4d$, $R_{H,0}$ can be determined from Norisuye's theory[96] based on a spherocylinder:

$$\frac{1}{R_{H,0}} = \frac{2}{L}[C_0 \ln \sigma + C_1 + C_2\lambda L + C_3(\lambda L)^2 + C_4(\lambda L)^3 + C_5(\lambda L)^4 + C_6(\lambda L)^5] \quad (20)$$

The coefficients C_i are given in ref 96. We plot the fits to R_H for all values of N_{sc}, f, and N_{bb} in Figure 4. This shows that the values calculated based on the WLCy model agrees well with the simulation data. We emphasize that this is an independent verification that involves no fitting. Equation 18 depends on $R_{H,0}$, which are calculated from eq 17 for $L > 4d$ and from eq 20 otherwise. The predictions from eq. 20 are shown by the dotted lines in Figure 4.

We are not aware of any prediction for intrinsic viscosity $[\eta]_0$ using the WLCy model; however, a "touched-bead" model that represents the cylinder as a chain of neighboring bead provides the following expression[97]

$$[\eta]_0 = \frac{6^{3/2}\langle S^2 \rangle^{3/2}\Phi_\infty}{M}\Gamma + \left(\frac{L}{d}\right)\frac{5\pi N_A d^3}{12} \quad (21)$$

DOI: 10.1021/acs.macromol.9b00363
Macromolecules 2019, 52, 4858−4874

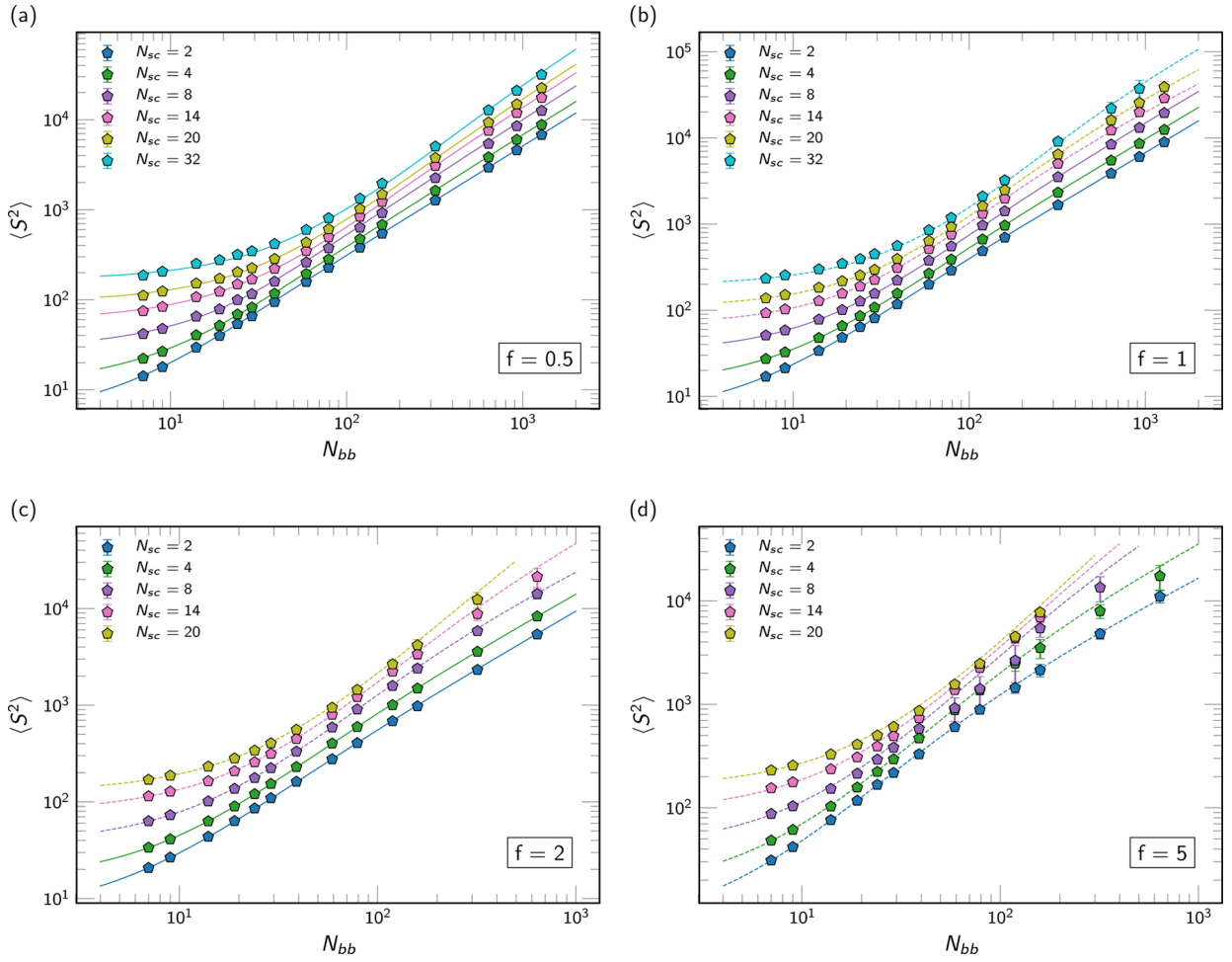

Figure 3. Mean-square radius of gyration $\langle S^2 \rangle$ as a function of backbone DP N_{bb} for different grafting densities: (a) $f = 0.5$, (b) $f = 1$, (c) $f = 2$, and (d) $f = 5$. Markers denote simulation data for the radius of gyration of the entire bottlebrush, solid lines denote fits considering the excluded volume interaction (eq 15), and dashed lines denote fits neglecting the effect of excluded volume (eq 14). Values of d used in these fits are tabulated in Tables 1–4, while other parameters (m_L, λ^{-1}, and B) were determined from matching $\langle R^2 \rangle$ in Figure 2.

where M is the molecular weight, $\Phi_\infty = 2.87 \times 10^{23}$ mol^{-1} is the Flory viscosity factor, N_A is the Avogadro's number, and

$$\frac{1}{\Gamma} = 1 + e^{-5\lambda L}[C_0 + C_1(\lambda L)^{1/2} + C_2\lambda L + C_3(\lambda L)^{3/2}] + e^{-1/4\lambda L}[C_4(\lambda L)^{-1/2} + C_5(\lambda L)^{-1} + C_6(\lambda L)^{-3/2} + C_7(\lambda L)^{-2}] \quad (22)$$

Here, the coefficients C_i are given in ref 97. This value can once more be modified using the QTP formalism[92] as

$$[\eta] = \alpha_\eta^3[\eta]_0 \quad (23)$$

where

$$\alpha_\eta^3 = (1 + 3.8\tilde{z} + 1.9\tilde{z}^2)^{3/10} \quad (24)$$

From eq 23, we calculate the reduced intrinsic viscosity $[\eta]M/\pi N_A a^3$ using the parameters as before. Note that the touched-bead model in eq 23 is subtly different than the WLCy model; the diameter in this context refers to the diameter of the touching beads constituting the cylinder and is not necessarily identical to d determined earlier based on a cylinder model. Similarly, the excluded volume parameter B is not necessarily identical to that determined based on a cylinder model. While a rigorous method would be to determine another set of d and B values only for intrinsic viscosity, we choose to retain d and modify B. We motivate this choice by noting that, for values of N_{sc} and f that do not use B, no change in d is needed to exhibit a nearly quantitative agreement between touched-bead predictions and simulation values of $[\eta]$. We find that substituting B with $B/2$ gives a good fit, as we can see from Figure 5. This factor of 1/2 is not entirely ad hoc, and a similar situation occurs for linear semiflexible chains as well, where the diameter of the touched-bead model is modified by a factor of 0.74 to match the predictions of the cylinder model.[97] Nevertheless, this is a known prefactor, albeit heuristically determined, and we feel it is unlikely to prevent application of the WLCy model for future purposes.

3.5. Form Factor. To obtain further insight into the conformations and semiflexible nature of bottlebrushes, we calculate the form factors of bottlebrush molecules for different side chain lengths, backbone lengths, and grafting densities. Figure 6 shows the form factor of the entire molecule and that of only the backbone for a long bottlebrush ($N_{bb} = 926$) at grafting density $f = 1$. Both form factors look very similar as that obtained by Yethiraj[28] from Monte Carlo simulations of single bottlebrushes. We indicate on Figure 6a the length scales associated with $q = \lambda$ and $q = 1/d$ as determined by the wormlike cylinder model parameterization, with a clear kink in the form factor at $q = 1/d$ that we interpret as connected to the

DOI: 10.1021/acs.macromol.9b00363
Macromolecules 2019, 52, 4858–4874

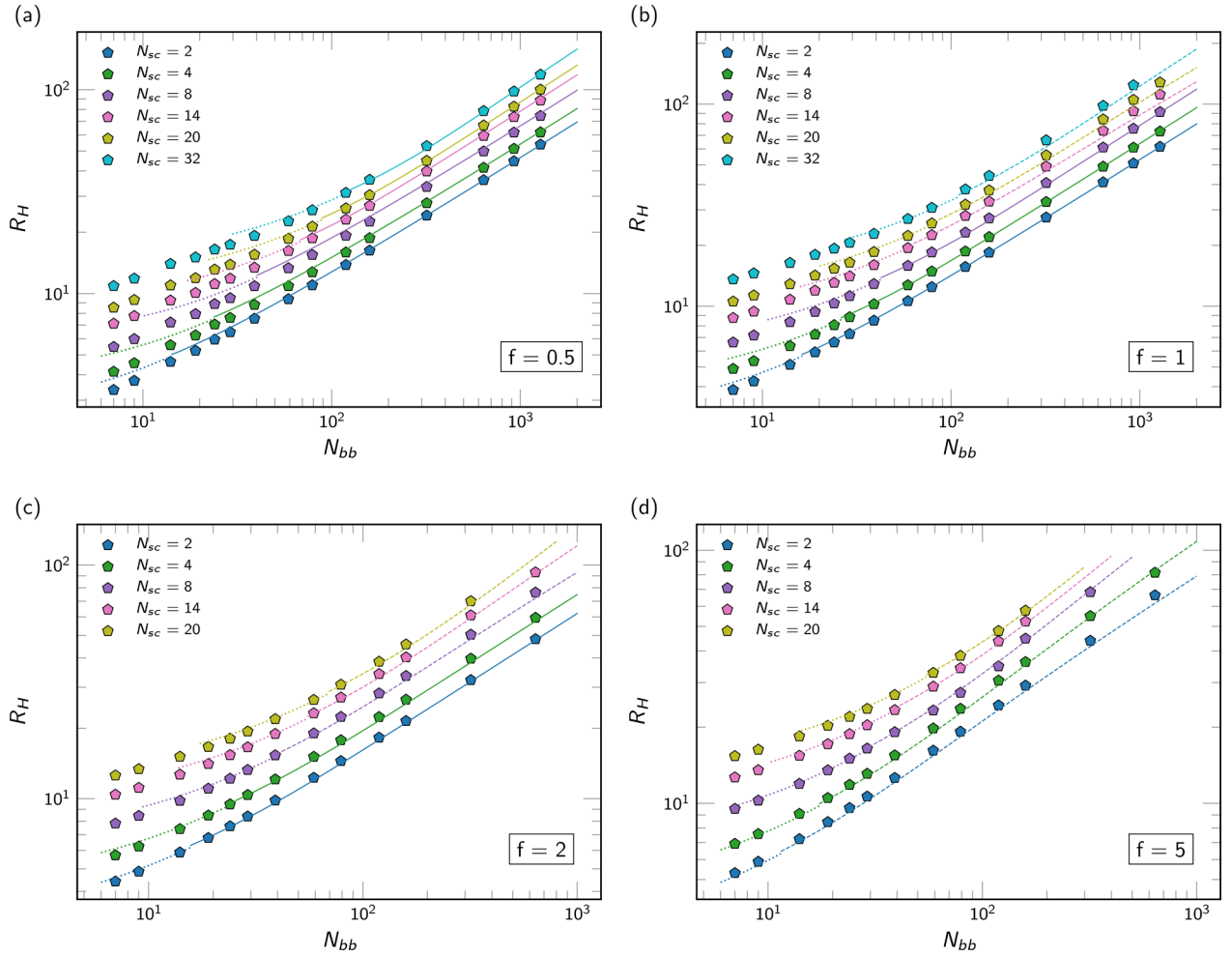

Figure 4. Hydrodynamic radius R_H as a function of backbone DP N_{bb} for different grafting densities: (a) $f = 0.5$, (b) $f = 1$, (c) $f = 2$, and (d) $f = 5$. Markers denote simulation data, solid lines denote values calculated considering the excluded volume interaction (eq 18), dashed lines denote values neglecting the effect of excluded volume (eq. 17, and dotted lines denote values calculated based on spherocylinder model (eq 20). The dotted lines are truncated at $L = d$, below which the spherocylinder model is no longer valid.

bottlebrush width. Further interpretation is challenging due to the absence of a suitable model for the overall bottlebrush form factor $P(qa)$, but the backbone form factor $P_{bb}(qa)$ is more readily amenable to interpretation. We observe the well-known power law decay of the form factor versus q for linear, with an exponent of −1.7. With an increase in side chain length, three regimes can be seen to emerge (see Figure 6b): (i) at small length scales (ca. 10 bond lengths), the local structure is the same as a linear chain; (ii) at intermediate length scales, $P_{bb} \approx q^{-1}$, indicating a rodlike structure; (iii) at longer length scales (but still shorter than the overall molecular size), the exponent m in $P_{bb} \approx q^m$, which is the slope in the log−log plot, changes from $m = -1$ toward the swollen coil-like limit of $m = -1.7$. We point out that, in Figure 6b, the slope of $m = -1$ becomes more apparent for higher N_{sc}; the change in slope from $m = -1$ to a lower value (i.e., toward −1.7) does not actually reach the limiting value of $m = -1.7$, indicating that the bottlebrushes are not sufficiently long to reach a flexible chain limit. Rodlike scaling over intermediate length scales have also been observed in simulations of bottlebrush molecules under melt conditions.[98] Form factors for many other values of N_{bb} and f are provided in the Supporting Information. We plot the form factors in Figure 6b as functions of the value λ as parameterized earlier in Figure 7. Here, we compare the backbone form factor P_{bb} with the theoretical predictions of Pedersen and Schurtenberger[99] for semiflexible chains. For $N_{sc} \leq 8$, we use the analytical expression (from ref 99 incorporating excluded volume; for $N_{sc} > 8$, the expression without excluded volume is used, in accordance with the data in Table 2. Once more, we observe consistency between the predictions emerging from the parameterized values (lines in Figure 7) and simulation data (points in Figure 7).

4. DISCUSSION

We were able to show that a wide variety of architectures (defined by N_{bb}, N_{sc}, and f) can be consistently fit to exhibit to a small number of parameters (m_L, λ^{-1}, B, and d) that quantitatively match, via the WLCy model, a number of different simulation observables ($\langle R^2 \rangle$, $\langle S^2 \rangle$, R_H, $[\eta]$, and $P(qa)$). This points to the success of the WLCy model as a tool to understand the behavior of explicit side chain simulations in the context of the overall molecular geometry and provides the basis to study the impact of molecular architecture on parameters such as the Kuhn length λ^{-1} and bottlebrush thickness d. This furthermore allows us to compare with our intuition on the bottlebrush structure and understand this same structure in the context of prior theory and simulation results.

DOI: 10.1021/acs.macromol.9b00363
Macromolecules 2019, 52, 4858−4874

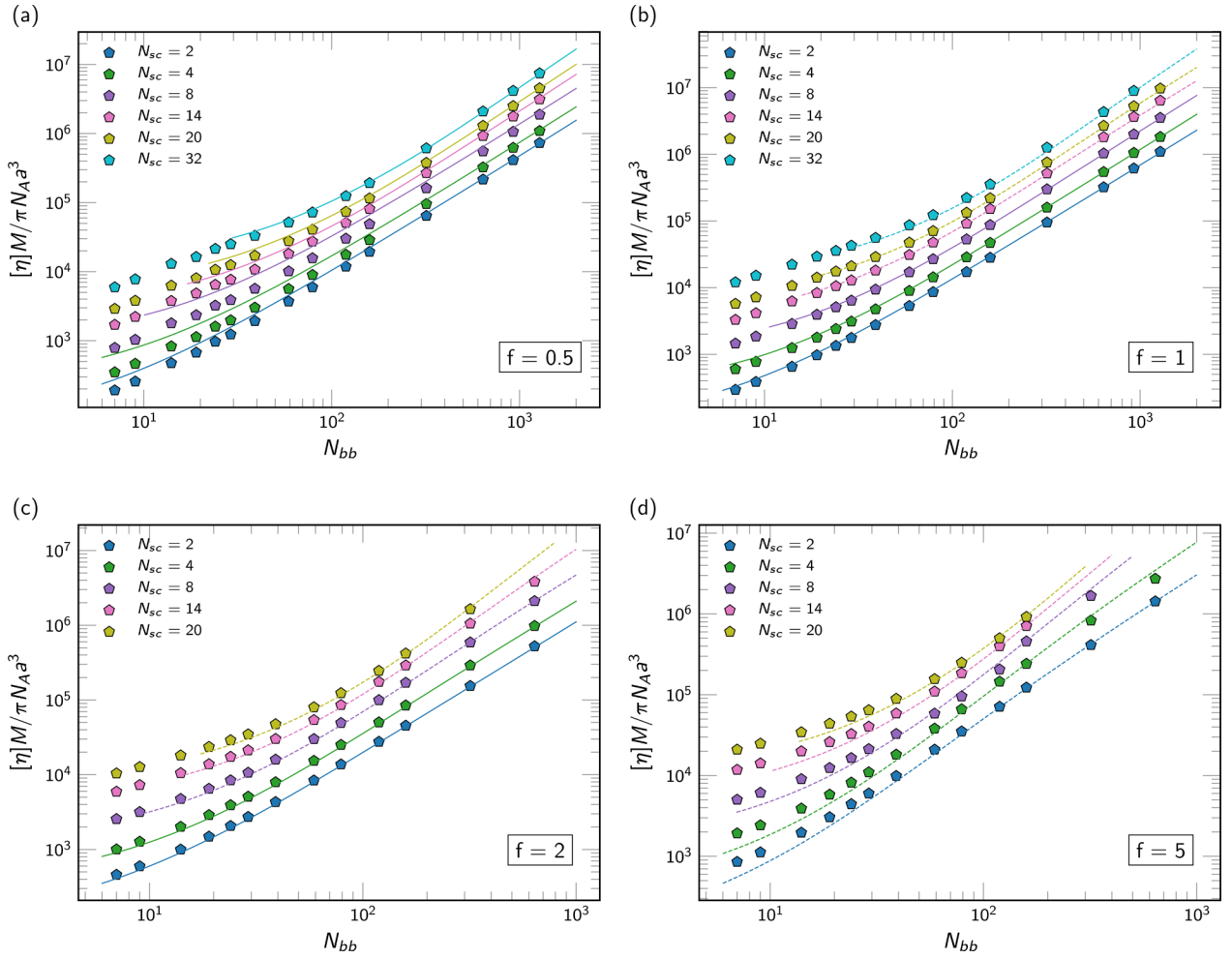

Figure 5. Intrinsic viscosity (reduced form) as a function of backbone DP N_{bb} for different grafting densities: (a) $f = 0.5$, (b) $f = 1$, (c) $f = 2$, and (d) $f = 5$. Markers denote simulation data, solid lines denote values calculated considering the excluded volume interaction (eq 23), and dashed lines denote fits neglecting the effect of excluded volume (eq 21). The lines are truncated at $L = d$, below which the touched-bead model is no longer valid.

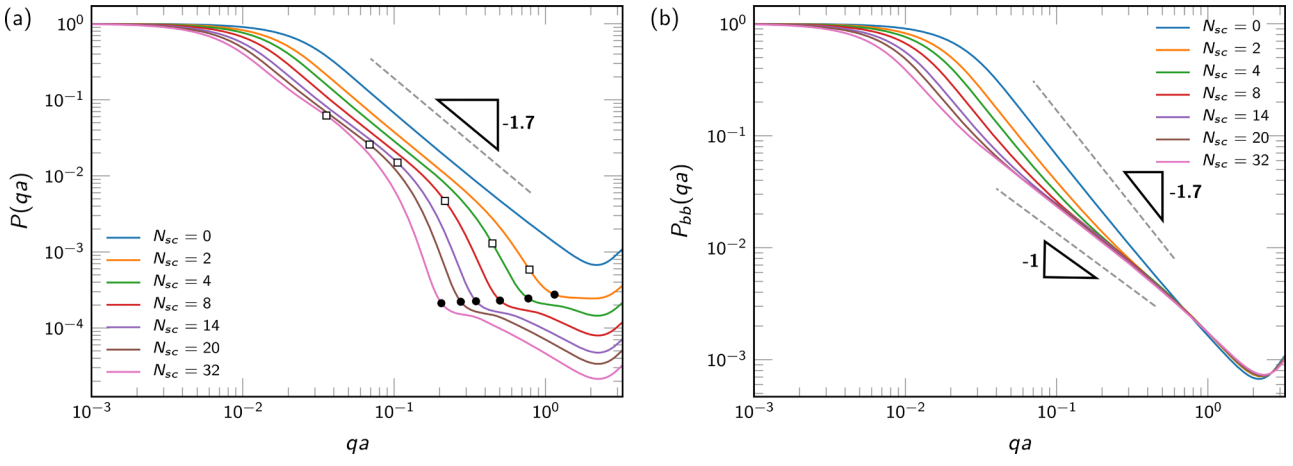

Figure 6. (a) Form factor of a bottlebrush molecule with $N_{bb} = 926$ and $f = 1$ for different side chain lengths. The black dots mark $1/d$, and the unfilled squares mark the persistence lengths $2/\lambda^{-1}$ (from Table 2). (b) Backbone form factor for the same molecule as in panel (a) showing the wormlike behavior on intermediate length scales. In both panel, $N_{sc} = 0$ denotes a linear chain.

4.1. Bottlebrush Length Is Shorter than Backbone Contour. For all values of m_L tabulated from Tables 1−4, the coarse-grained contour length is less than the contour length calculated from the actual number of backbone bonds and the equilibrium bond length. As pointed out in an earlier experimental work[100] and simulation work,[28] the backbone can bend over smaller length scales that do not manifest in the overall molecular geometry of the bottlebrush. Indeed, this

DOI: 10.1021/acs.macromol.9b00363
Macromolecules 2019, 52, 4858−4874

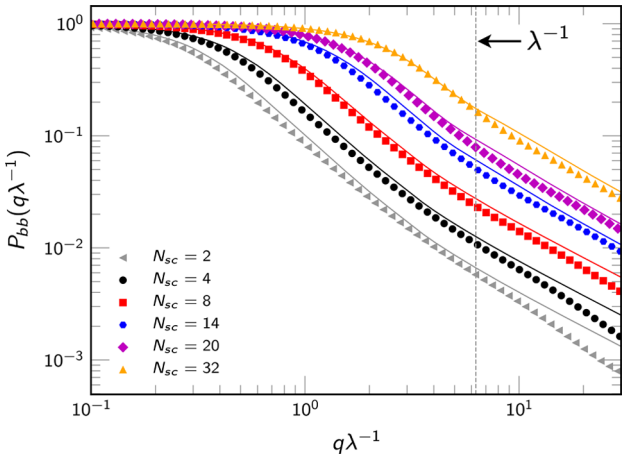

Figure 7. Backbone form factor of a bottlebrush molecule with N_{bb} = 926 and f = 1 for different side chain lengths (denoted by markers) compared to the theoretical predictions (solid lines) for a wormlike chain from ref 99 using parameters from Table 2.

effect is extremely pronounced at lower grafting densities, f = 1 and f = 1/2, where the value of m_L decreases with N_{sc}. We attribute this to the decreased ability of fluctuations in the bottlebrush backbone to persist to the "edge" of the bottlebrush structure as the length of the side chains increases. At higher grafting densities, f = 2 and f = 5, the value of m_L becomes insensitive to N_{sc}, which is consistent with light scattering measurements from Terao et al.[63]

4.2. Side Chains Set the Diameter of the Bottlebrush.

The value of d determined by the WLCy model is consistent with the intuition that it should be set by the length of the side chains N_{sc}. This is plotted in Figure 8a, which plots d versus N_{sc} on a log–log plot. The observed scaling is very similar for all values of f considered here, with $d \approx N_{sc}^{0.62}$. This scaling exponent of 0.62 is close to that of linear flexible chains but is slightly higher, which we attribute to modest side chain stretching. Indeed, this stretching appears to quantitatively increase with f, which shows a monotonic increase in d. This appears to be a small effect of d; however, we note that the log scale does not do justice to the extent of this change; quantitative values from Tables 1 and 4 show that at N_{sc} = 20 there is a ≈25% increase in the value of d as f is increased from f = 1/2 to f = 5.

In addition to this architectural comparison, we also note that the geometric value d corresponds well with measures of side chain structure such as the side chain radius of gyration $\langle S_{sc}^2 \rangle$. d is is plotted in Figure 8b as a function of $\langle S_{sc}^2 \rangle$ for all values of f, and the correlation between the two values is extremely close, with small deviations occuring only at small values of d (i.e., small side chain lengths). The correlation is not quite linear, however, with a scaling exponent of 1.07. The agreement between d, $\langle S_{sc}^2 \rangle^{1/2}$, and N_{sc} provides a consistency check for the WLCy model and agrees with the intuition that side chains govern the bottlebrush diameter. As an additional point, we note that B also correlates with d and N_{sc}; this is expected, since it reflects the excluded volume of the chain, but there are not enough bottlebrush runs with $B > 0$ to draw any major conclusions.

4.3. Side Chains Set the Flexibility of the Bottlebrush.

Extensive simulation and theory work in the literature has studied the connection between the stiffness of a bottlebrush and the length and density of the side chains. There remains some controversy in this area due to the challenges of ascribing a persistence length or Kuhn length λ^{-1} that is not intrinsic to the chemistry of the molecule but rather the statistical interactions between architectural features. A major concern is that the effective persistence length is often (i) dependent on the length of the chain backbone N_{bb} and, (ii) if defined locally, varies over the contour of the bottlebrush and consequently depends on the length of the backbone N_{bb}.[30,36,101]

The fits to the WLCy model in Tables 1–4 provide predictions for how λ^{-1} changes as a function of the chain architecture. We find that λ^{-1} increases with N_{sc}, with values for f = 1 and f = 1/2 ranging from 11 to ca. 300. This is within the range of Kuhn lengths reported in the experiments.[61,77−80] This connection between Kuhn length λ^{-1} and N_{sc} is plotted in Figure 9a as solid points and lines. Comparing the data for each N_{sc} on increasing grafting density, we match the intuitive expectations that denser grafting should lead to higher stiffness.

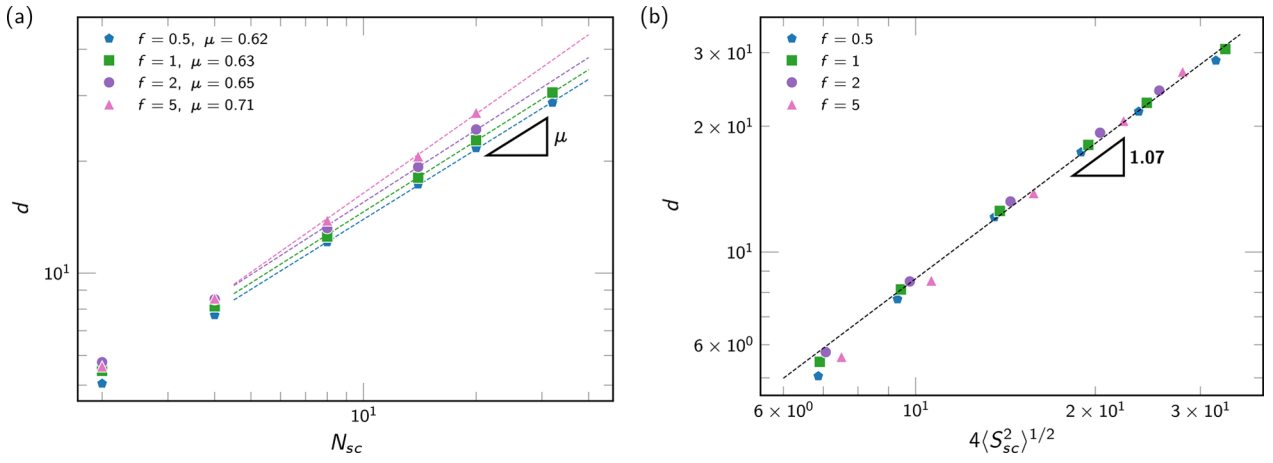

Figure 8. (a) WLCy diameter d versus side chain DP N_{sc} for different grafting densities f. Scaling exponent μ is indicated, showing increased side chain stretching away from the ideal chain value μ = 0.588 as f is increased. (b) WLCy diameter d versus side chain radius of gyration $\langle S_{sc}^2 \rangle^{1/2}$ for different grafting densities. All values of f fall roughly along the same correlation, demonstrating that the parameterized value d reflects the local conformation geometry of the side chains.

DOI: 10.1021/acs.macromol.9b00363
Macromolecules 2019, 52, 4858−4874

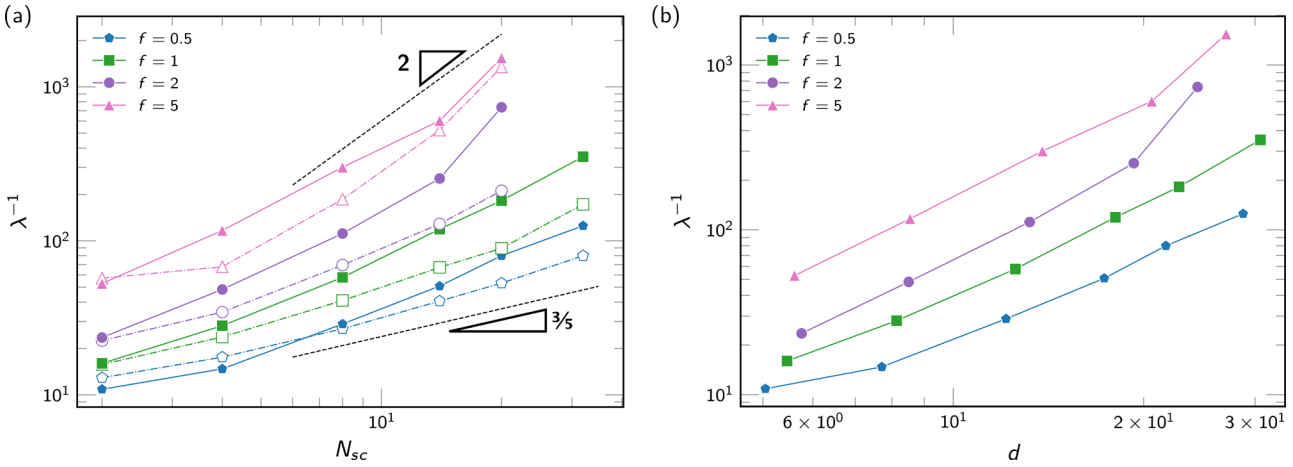

Figure 9. (a) Kuhn length λ^{-1} as a function side chain degree of polymerization N_{sc} and grafting density f. Solid markers denote predictions based on the WLCy model, while open markers denote values calculated from eq 25, which is from Cao et al.[47] We note that, at low N_{sc}, there is an excellent agreement; however, the two results deviate at large N_{sc}. (b) Kuhn length λ^{-1} as a function of diameter d for different grafting densities f, demonstrating that thick bottlebrushes exhibit a significant increase in chain stiffness.

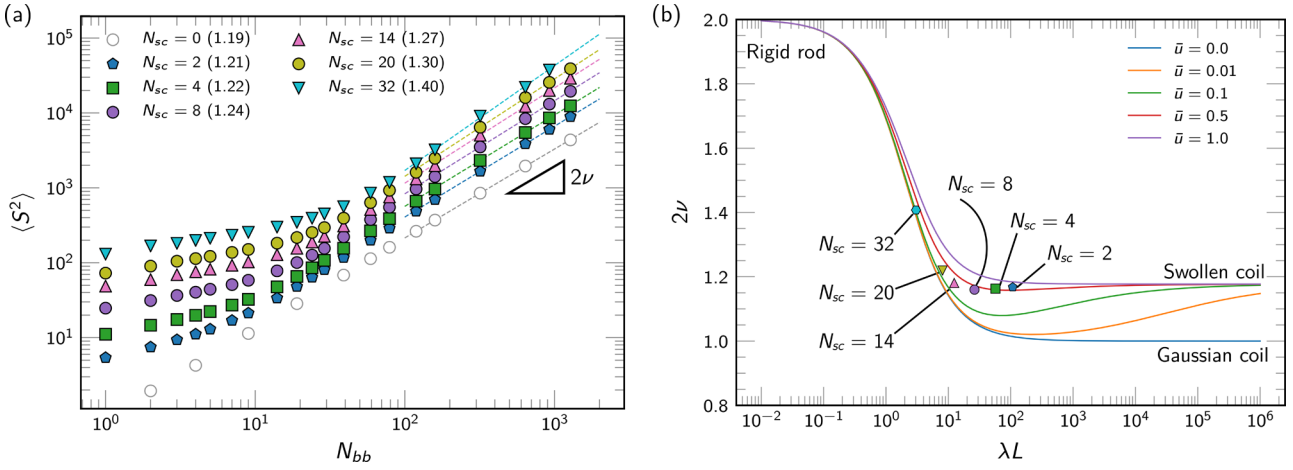

Figure 10. (a) Mean-square radius of gyration as a function of backbone DP for different side chain DPs at grafting density $f = 1$. The label $N_{sc} = 0$ denotes a linear chain. Scaling exponents 2ν are shown within parentheses for each value of N_{sc}. (b) Scaling exponent as a function of rescaled contour length as predicted from the renormalization group theory[106] for different values of the rescaled excluded volume parameter $\bar{u}$. Markers denote the longest bottlebrush considered in panel (a) for each value of N_{sc}.

These simulation/WLCy determinations for λ^{-1} can be compared to a number of theoretical and simulation predictions in the literature to determine the extent that our predictions are consistent or inconsistent with other types of models. We first compare λ^{-1} determined from the WLCy model with that calculated using eq. 6 from ref 47. In that work, the equation

$$\frac{1}{\lambda} = b\left[(1-\alpha)\frac{1+e^{-1/\lambda_1}}{1-e^{-1/\lambda_1}} + \alpha\frac{1+e^{-1/\lambda_2}}{1-e^{-1/\lambda_2}}\right] \quad (25)$$

uses the fitting parameters α, λ_1, and λ_2, which are obtained from the backbone bond correlation function via the expression

$$G(l) = (1-\alpha)e^{-l/\lambda_1} + \alpha e^{-l/\lambda_2}$$

and b is the bond length. The two exponentials are intended to capture the fast and slow decay of the orientation of the backbone bonds. Similar models for backbone orientational decay have been found to be applicable in the case of polyelectrolytes.[102] We plot λ^{-1} calculated from eq 25 versus N_{sc} in Figure 9a with open symbols and dashed lines. While both are similar qualitatively, λ^{-1} from the WLCy model is much higher quantitatively, though the deviation almost completely disappears at low N_{sc}. We attribute this disparity to a number of reasons related to the challenges of using simulation to calculate λ^{-1}. First, we note that the value of λ^{-1} calculated from eq 25 exhibits a slow increase with an increase in N_{bb}; this variation has been reported in the work by Hsu et al. as a pitfall of using the backbone bond correlation.[30] By contrast, the WLCy model ascribes a single value of λ^{-1} to the entire range of N_{bb} values, resulting in an excellent fit that is consistent over a wide range of observables. Second, and perhaps more fundamentally, we noted earlier that the conformational behavior of the backbone is not the same as the overall geometry of the bottlebrush. This was previously discussed in the context of m_L, but we suggest the same is true for λ^{-1}, and that the stiffness of the backbone does not track completely with the stiffness of the bottlebrush structure. This is consistent with the nature of the deviations seen in Figure 9a, which grow significantly as the value of N_{sc} is increased; in this limit, as in our discussion of m_L, the overall bottlebrush

DOI: 10.1021/acs.macromol.9b00363
Macromolecules 2019, 52, 4858−4874

structure is least sensitive to the behavior of the backbone chain conformation. We finally note that eq 25 was intended for bottlebrush melts, where the excluded volume interactions are negligible.

We can also frame our predictions from the simulation and WLCy theory in terms of the scaling arguments made in the literature. Fredrickson,[57] Subbotin et al.,[103] and Nakamura and Norisuye[104] have argued, based on the scaling theory, that $\lambda^{-1} \approx N_{sc}^2$ at sufficiently high grafting density. By contrast, Birshtein et al.[56] proposed, in an alternative theory, that $\lambda^{-1} \approx D \approx N_{sc}^{3/5}$, which approaches that of a self-avoiding walk. Other theories also exist with intermediate predictions.[34,58] To compare with these scaling theories, we have indicated the slopes of 3/5 and 2 in Figure 9a. While our side chains are not long enough to draw specific conclusions on this point, it appears that both predictions may be observed at the corresponding limits of low or high grafting density and our simulations are largely in a transition regime between the two physical arguments.

Figure 9b shows the dependence of λ^{-1} on d. While we again find no clear indication of an unambiguous scaling law, it is interesting to note that λ^{-1} is typically much larger than d. This contrasts with the prediction of Birshtein et al.[56] that the Kuhn length is of the same order as d. Furthermore, it is predicted[105] that to obtain lyotropic ordering $\lambda^{-1}/d \geq 10$. This is indeed true for higher values of N_{sc} even at $f = 1$, as can be seen from Figure 9b and Table 2. Lyotropic ordering of bottlebrushes has been previously reported in the literature,[19−21] confirming that the WLCy model parameters are in the appropriate regimes suitable for reproducing experimental observations.

4.4. WLCy Parameters Consistent with Scaling Exponents in a Crossover Regime. We have demonstrated that the WLCy model is consistent with fine-grained, explicit side chain simulations. This demonstrates that it is possible to place the conformational behavior of bottlebrushes in the context of known behaviors for standard semiflexible polymer chains with finite thickness. Figure 10a shows the scaling of the mean-square radius of gyration for different side chain lengths with respect to backbone DP for $f = 1$, similar to Figure 3b but now including the linear chain (open symbols) and denoting the scaling exponent 2ν. We observe that 2ν slightly increases with an increase in N_{sc}, with small N_{sc} still quite close to the asymptotic scaling exponent of $2\nu \approx 1.2$ predicted for flexible linear chains,[92] but larger N_{sc} increases notably to $2\nu \approx 1.4$. This prediction is similar to prior simulation results for bottlebrushes with flexible backbone.[28,40]

These scaling observations can be placed in the context of calculations for wormlike polymer chains from the renormalization group theory of Chen and Noolandi.[106] Here, the scaling exponent 2ν is a function of both the rescaled contour length λL and the dimensionless excluded volume parameter $\bar{u}$, which is defined as $\bar{u} = \frac{\lambda w}{0.1777}\left(\frac{2\pi}{3}\right)^{-3/2}$. Here, w is an effective diameter of a segment impenetrable by other segments.[106] Figure 10b plots the scaling exponent 2ν for various values of $\bar{u}$. The absence of excluded volume corresponds to $\bar{u} = 0$. In this case, $2\nu \to 1$ as $\lambda L \to \infty$, in accordance to the behavior of Gaussian chains. When $\bar{u} \neq 0$, $2\nu \to 1.16$ as $\lambda L \to \infty$, corresponding to the behavior of excluded volume chains. This graph quantitatively captures the crossovers governing the standard scaling understanding of semiflexible polymers; when the polymer is significantly shorter than the persistence length ($\lambda L \ll 1$), the chain is rodlike. As the polymer increases in length, with weak excluded volume, it will exhibit Gaussian statistics, and eventually the excluded volume interaction energy becomes sufficiently large to swell the coil. It is is possible to avoid the intermediate Gaussian regime at large values of $\bar{u}$. Beyond these conceptual scaling regimes, however, it should be noted that there are large crossover regimes where the chain is not fully rodlike, Gaussian, or swollen; this has been crucial to understanding other semiflexible chains such as DNA.[107]

We show that the WLCy parameters determined from explicit solvent simulations fall squarely in these crossover regimes. We use the value of λL corresponding to the longest bottlebrush for each N_{sc} plotted in Figure 10a ($f = 1$) and use $w = d$ calculated for the same bottlebrushes. This choice is made for the sake of simplicity, as it allows us to place our results in the context of the existing renormalization group theory; we do note that it is unclear that this choice of $w = d$ is quantitatively appropriate when the width dimension is dictated by the polymer architecture. Nevertheless, it enables us to predict, from the renormalization group theory, the value of 2ν, which is plotted in Figure 10b and qualitatively similar to the exponents indicated in Figure 10a, spanning $2\nu \approx 1.2-1.4$ and increasing with increasing N_{sc}. We note that there are some quantitative differences, which we attribute to our choice to relate w to d rather than B; this is done in part because d is accessible for the entire range of values N_{sc}, while B cannot be accurately determined for large N_{sc}. We expect the general trend to hold, however, with the use of d slightly underestimating $\bar{u}$ when compared to the exponents indicated in Figure 10a. This is consistent with the observation that $B > d$. The key observation from Figure 10b is that the values of 2ν are indeed in the crossover regime between the rodlike, swollen coil, and Gaussian coil regimes. At large values of N_{sc} (e.g., $N_{sc} = 32$), the value of $\bar{u} \to 0.0$ and a sufficiently long bottlebrush would be expected to exhibit Gaussian statistics at some intermediate length. At short side chain lengths (i.e., $N_{sc} \approx 2 - 8$), the system exhibits chain statistics close to that of a swollen coil. However, none of the examples shown are fully in one of the asymptotic scaling regimes.

5. USING THE WLCY MODEL TO COARSE-GRAIN POLYMER CHAINS

The success of the WLCy model to describe explicit side chain, fine-grained molecular models suggests that it is possible to use an equivalent touched-bead model with implicit side chains to represent bottlebrush polymers. Indeed, a semianalytical version of such a model was already used with success[97] in describing intrinsic viscosity $[\eta]$. We thus introduce a discretized wormlike cylinder (DWLCy) model, where the bottlebrush is modeled as a string of touched beads and the Stokes radius of each bead is equal to the diameter d of the corresponding WLCy model.

We use the same Brownian dynamics method described earlier in Section 2 for the fine-grained models, only now the connectivity is modeled with a simple Hookean spring energy $U_s = -\sum_{i,j} {}^*k_s(r_{ij} - 1)^2/2$, where $k_s = 200\varepsilon/\sigma^2$. The bending potential is still given by eq 3, only now with $k_b = (2\lambda d)^{-1}$ to reflect the values of d and λ determined from the WLCy model. In contrast to the $O(10^4)$ beads needed for single-molecule simulations of the explicit side chain bottlebrush, these new implicit side chain simulations are run with a total number of 3−240 beads. We perform the simulations both with and without considering excluded volume effects. For

DOI: 10.1021/acs.macromol.9b00363
Macromolecules 2019, 52, 4858−4874

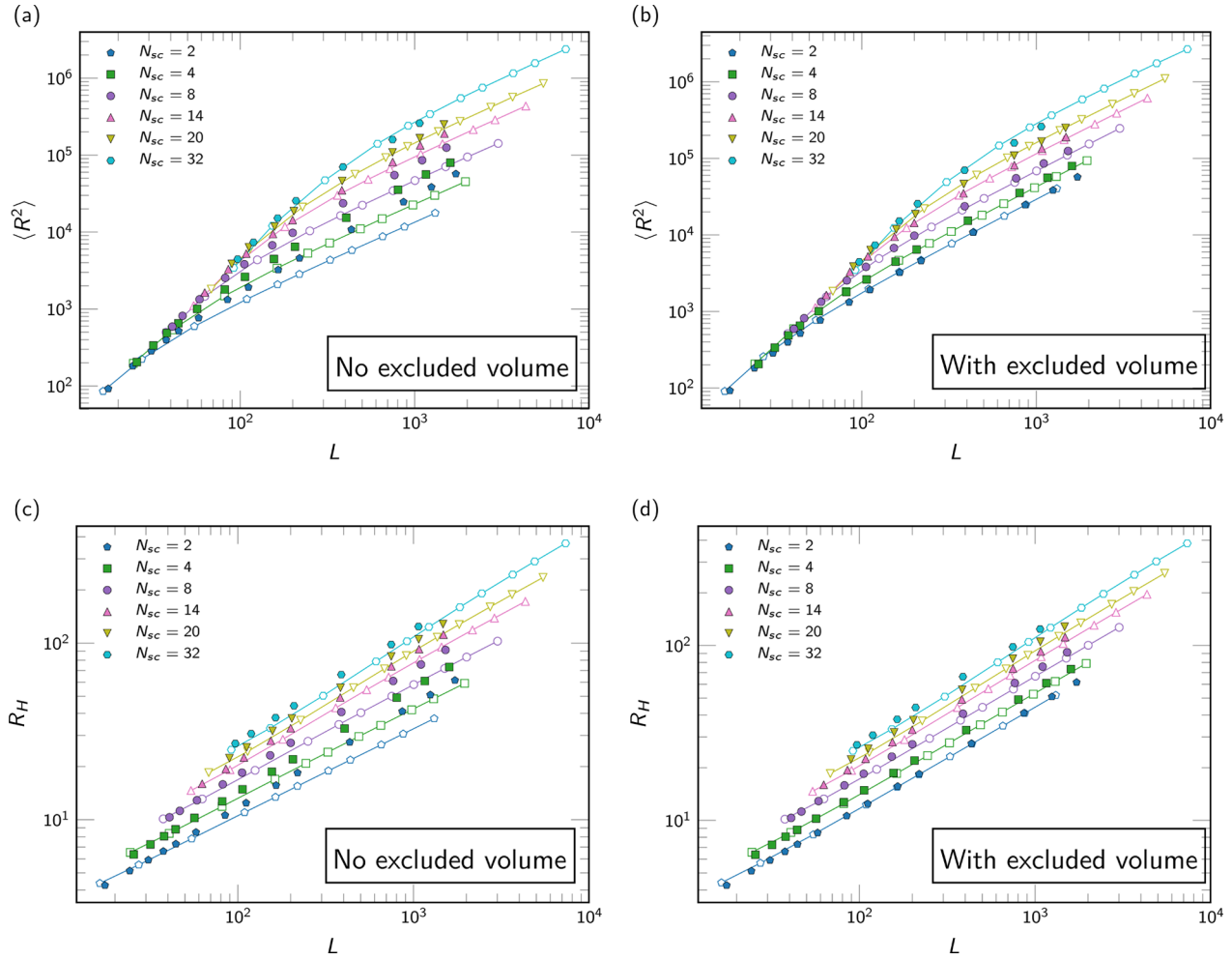

Figure 11. Mean-square end-to-end distance (a) without and (b) with excluded volume and hydrodynamic radius (c) without and (d) with excluded volume as a function of contour length L for different side chain lengths at grafting density $f = 1$. Unfilled markers are data from simulations using coarse-grained touched-bead models, and filled markers are data from simulations using fine-grained bead-spring models. Lines are meant to guide the eye.

simulations with excluded volume, a potential of the same form as eq 2 was used with the length parameter σ equal to the diameter d as determined from the WLCy model. We specifically note that this choice of $d = \sigma$ represents a loss in a degree of freedom, that is, d and B are no longer independent as they are in the WLCy model. Here, σ is related to the quantity B as the characteristic length scale of the excluded volume potential. This loss in independence is reflected in the inability to find a single value of σ that consistently fits for all N_{sc}; Figure S8 in the Supporting Information shows how different choices for σ can be parameterized to more accurately fit different values of N_{sc}. It is thus likely appropriate to choose a value of $d \neq \sigma$, which reflects the independence of the value B; however, we do not explore this choice in this manuscript.

Figure 11 shows the comparison between the explicit (filled symbols) and implicit (open symbols) side chain simulations for $f = 1$, all values of N_{sc}, and observables $\langle R^2 \rangle$ and R_H. The effect of excluded volume on the implicit side chains is also shown. Similar plots for $\langle S^2 \rangle$ and $[\eta]$ are provided in the Supporting Information. There is good agreement between both simulations when excluded volume is considered; even in the absence of excluded volume, the agreement is nearly quantitative for $N_{sc} \geq 14$, which corresponds to systems where B was not required for parameterization. We note that, while the implicit side chain model is not suitable for backbone lengths of the same order as the diameter, it becomes progressively useful as the bottlebrush grows longer compared to its diameter as these simulations are capable of accessing bottlebrushes about an order of magnitude longer in length than the explicit side chain simulations. This demonstrates the computational benefit of these simulations, though we emphasize that the plotted values were not an attempt to obtain the maximum bottlebrush length accessible to simulation; we expect the true computational limit is at significantly longer bottlebrush lengths. We do note that low values of N_{sc} exhibit deviations between the explicit and implicit side chain simulations. This is of course due to the lack of excluded volume in the implicit side chain simulations, because deviations occur precisely where the QTP model for excluded volume becomes important in the WLCy fits. These chains are expected to swell and move significantly closer to the explicit side chain results upon inclusion of an excluded volume potential.

6. CONCLUSIONS

In this paper, we demonstrated that the wormlike cylinder (WLCy) model can be systematically parameterized to describe bottlebrush polymers with flexible backbone and

DOI: 10.1021/acs.macromol.9b00363
Macromolecules 2019, 52, 4858−4874

side chains in dilute solution. This parameterization was performed using explicit side chain models for bottlebrush polymers that are known to match well with experimental data, thus allowing us to develop a coarse-grained representation of synthesized bottlebrush polymers. The WLCy model was demonstrated to be internally consistent among a number of molecular observables, including end-to-end distance, radius of gyration, hydrodynamic radius, and intrinsic viscosity, with parameterization from two of these values predicting the other two almost quantitatively.

This parameterization provided insight into the molecular structure of bottlebrush polymers, matching qualitatively with the previous theory and simulation of these molecules. In the context of the WLCy model, we can understand a number of physical aspects of bottlebrush molecules, capturing how the molecular length relates to the backbone contour, how side chains affect the bottlebrush diameter, and how the same side chains set the bottlebrush flexibility. We can also compare to classical renormalization group calculations to demonstrate that the overall bottlebrush conformation exists in a crossover regime of wormlike polymer behavior, with the molecular size exhibiting intermediate scaling exponents between the rodlike, Gaussian, and swollen coil limits. The location within this crossover regime is determined both by the molecular length and the length of the side chains, which affect both the flexibility and width of the bottlebrush.

Finally, we show that the WLCy model enables the development of coarse-grained implicit side chain simulation models, which represent a significant computational speedup over explicit side chain representations. We show nearly quantitative agreement between the two models and also that much longer bottlebrush molecules can be simulated for the implicit side chain model.

The success of the WLCy model sets the stage for using computation to understand the behavior of bottlebrush suspensions, where nondilute bottlebrushes exhibit nontrivial rheological response and molecular self-assembly. This leads to a number of open questions for bottlebrush modeling, such as, can we further decrease the number of parameters needed for the coarse-graining by relating, for example, d and B and d and λ^{-1}, in an accurate fashion. In principle, the former should already be possible using statistical mechanical arguments; however, we are limited in the data for B due to the stiffness of the bottlebrushes we have considered. We also expect the modeling of excluded volume in the implicit side chain models to be nontrivial but important; this is key for single-chain effects such as the deviations in Figure 11 but also for the inter-bottlebrush interactions that will occur in nondilute bottlebrush solutions. We expect that comparison to experimental data, which already exhibits excellent matching to these simulations in dilute solution,[52] will be crucial to parameterizing excluded volume effects in nondilute solutions. Further simulation study, for example, capturing the potential of mean force between the two bottlebrush molecules, would also aid in the parameterization and understanding of excluded volume when it arises due to densely grafted macromolecules. Ultimately, we would like to extend this model beyond homopolymer, cylindrical bottlebrushes to consider bottlebrush block copolymers[54,108−111] and bottlebrushes with noncylindrical geometries.[112,113]

■ ASSOCIATED CONTENT

Supporting Information

The Supporting Information is available free of charge on the ACS Publications website at DOI: 10.1021/acs.macromol.9b00363.

Bottlebrush form factor P and backbone form factor P_{bb} at grafting densities f = 0.5, 1, 2, and 5 for different side chain lengths and backbone lengths; comparison of backbone form factor to the wormlike chain theory; fits to mean-square radius of gyration excluding and including the B parameter at f = 1; mean-square radius of gyration with and without excluded volume and reduced intrinsic viscosity with and without excluded volume as a function of contour length L for different side chain lengths at grafting density f = 1; and comparison of mean-square end-to-end distance between simulations using a fine-grained model and that using the DWLCy model at f = 1 (PDF)

■ AUTHOR INFORMATION

Corresponding Author

*E-mail: cesing@illinois.edu.

ORCID

Sarit Dutta: 0000-0002-6197-7881

Charles E. Sing: 0000-0001-7231-2685

Notes

The authors declare no competing financial interest.

■ ACKNOWLEDGMENTS

This work was supported by the National Science Foundation under DMREF award number DMR-1727605. The authors thank Simon Rogers, Damien Guironnet, Ying Diao, Matthew Wade, Ching-Wei Lee, Dylan Walsh, Jaimie Kurtz, and Bijal Patel for intellectual discussions regarding this work.

■ REFERENCES

(1) Xie, G.; Martinez, M. R.; Olszewski, M.; Sheiko, S. S.; Matyjaszewski, K. Molecular Bottlebrushes as Novel Materials. *Biomacromolecules* **2018**, *20*, 27−54.

(2) Sveinbjörnsson, B. R.; Weitekamp, R. A.; Miyake, G. M.; Xia, Y.; Atwater, H. A.; Grubbs, R. H. Rapid Self-Assembly of Brush Block Copolymers to Photonic Crystals. *Proc. Natl. Acad. Sci. U. S. A.* **2012**, *109*, 14332−14336.

(3) Saito, Y.; Kikuchi, M.; Jinbo, Y.; Narumi, A.; Kawaguchi, S. Determination of the Chain Stiffness Parameter of Molecular Rod Brushes Consisting of a Polymethacrylate Main Chain and Poly(N-Hexyl Isocyanate) Side Chains. *Macromolecules* **2015**, *48*, 8971−8979.

(4) Liberman-Martin, A. L.; Chu, C. K.; Grubbs, R. H. Application of Bottlebrush Block Copolymers as Photonic Crystals. *Macromol. Rapid Commun.* **2017**, *38*, 1700058.

(5) Aluculesei, A.; Pipertzis, A.; Piunova, V. A.; Miyake, G. M.; Floudas, G.; Fytas, G.; Grubbs, R. H. Thermomechanical Behavior and Local Dynamics of Dendronized Block Copolymers and Constituent Homopolymers. *Macromolecules* **2015**, *48*, 4142−4150.

(6) Sun, F.; Sheiko, S. S.; Möller, M.; Beers, K.; Matyjaszewski, K. Conformational Switching of Molecular Brushes in Response to the Energy of Interaction with the Substrate. *J. Phys. Chem. A* **2004**, *108*, 9682−9686.

(7) Xu, H.; Sun, F. C.; Shirvanyants, D. G.; Rubinstein, M.; Shabratov, D.; Beers, K. L.; Matyjaszewski, K.; Sheiko, S. S. Molecular pressure sensors. *Adv. Mater.* **2007**, *19*, 2930−2934.

(8) Arrington, K. J.; Radzinski, S. C.; Drummey, K. J.; Long, T. E.; Matson, J. B. Reversibly Cross-Linkable Bottlebrush Polymers as

DOI: 10.1021/acs.macromol.9b00363
Macromolecules 2019, 52, 4858−4874

Pressure-Sensitive Adhesives. *ACS Appl. Mater. Interfaces* **2018**, *10*, 26662−26668.
(9) Lee, H.-i.; Boyce, J. R.; Nese, A.; Sheiko, S. S.; Matyjaszewski, K. pH-Induced Conformational Changes of Loosely Grafted Molecular Brushes Containing Poly(Acrylic Acid) Side Chains. *Polymer* **2008**, *49*, 5490−5496.
(10) Lee, H.-i.; Pietrasik, J.; Sheiko, S. S.; Matyjaszewski, K. Stimuli-responsive molecular brushes. *Prog. Polym. Sci.* **2010**, *35*, 24−44.
(11) Cai, L.-H.; Kodger, T. E.; Guerra, R. E.; Pegoraro, A. F.; Rubinstein, M.; Weitz, D. A. Soft Poly(Dimethylsiloxane) Elastomers from Architecture-Driven Entanglement Free Design. *Adv. Mater.* **2015**, *27*, 5132−5140.
(12) Vatankhah-Varnoosfaderani, M.; Daniel, W. F. M.; Zhushma, A. P.; Li, Q.; Morgan, B. J.; Matyjaszewski, K.; Armstrong, D. P.; Spontak, R. J.; Dobrynin, A. V.; Sheiko, S. S. Bottlebrush Elastomers: A New Platform for Freestanding Electroactuation. *Adv. Mater.* **2017**, *29*, 1604209−7.
(13) Vatankhah-Varnosfaderani, M.; Daniel, W. F. M.; Everhart, M. H.; Pandya, A. A.; Liang, H.; Matyjaszewski, K.; Dobrynin, A. V.; Sheiko, S. S. Mimicking Biological Stress−Strain Behaviour with Synthetic Elastomers. *Nature* **2017**, *549*, 497−501.
(14) Vatankhah-Varnosfaderani, M.; Keith, A. N.; Cong, Y.; Liang, H.; Rosenthal, M.; Sztucki, M.; Clair, C.; Magonov, S.; Ivanov, D. A.; Dobrynin, A. V.; Sheiko, S. S. Chameleon-Like Elastomers with Molecularly Encoded Strain-Adaptive Stiffening and Coloration. *Science* **2018**, *359*, 1509−1513.
(15) Liang, H.; Sheiko, S. S.; Dobrynin, A. V. Supersoft and Hyperelastic Polymer Networks with Brushlike Strands. *Macromolecules* **2018**, *51*, 638−645.
(16) Namba, S.; Tsukahara, Y.; Kaeriyama, K.; Okamoto, K.; Takahashi, M. Bulk Properties of Multibranched Polystyrenes from Polystyrene Macromonomers: Rheological Behavior I. *Polymer* **2000**, *41*, 5165−5171.
(17) Sheiko, S. S.; Sumerlin, B. S.; Matyjaszewski, K. Cylindrical Molecular Brushes: Synthesis, Characterization, and Properties. *Prog. Polym. Sci.* **2008**, *33*, 759−785.
(18) Rzayev, J. Molecular Bottlebrushes: New Opportunities in Nanomaterials Fabrication. *ACS Macro Lett.* **2012**, *1*, 1146−1149.
(19) Tsukahara, Y.; Ohta, Y.; Senoo, K. Liquid Crystal Formation of Multibranched Polystyrene Induced by Molecular Anisotropy Associated with its High Branch Density. *Polymer* **1995**, *36*, 3413−3416.
(20) Wintermantel, M.; Fischer, K.; Gerle, M.; Ries, R.; Schmidt, M.; Kajiwara, K.; Urakawa, H.; Wataoka, I. Lyotropic Phases Formed by"Molecular Bottlebrushes". *Angew. Chem., Int. Ed. Engl.* **1995**, *34*, 1472−1474.
(21) Rathgeber, S.; Pakula, T.; Wilk, A.; Matyjaszewski, K.; Lee, H.-i.; Beers, K. L. Bottle-brush macromolecules in solution: Comparison between results obtained from scattering experiments and computer simulations. *Polymer* **2006**, *47*, 7318−7327.
(22) Hsu, H.-P.; Paul, W.; Binder, K. One- and Two-Component Bottle-Brush Polymers: Simulations Compared to Theoretical Predictions. *Macromol. Theory Simul.* **2007**, *16*, 660−689.
(23) Saariaho, M.; Ikkala, O.; ten Brinke, G. Molecular Bottle Brushes in Thin Films: An off-Lattice Monte Carlo Study. *J. Chem. Phys.* **1999**, *110*, 1180−1187.
(24) Saariaho, M.; Subbotin, A.; Szleifer, I.; Ikkala, O.; ten Brinke, G. Effect of Side Chain Rigidity on the Elasticity of Comb Copolymer Cylindrical Brushes: A Monte Carlo Simulation Study. *Macromolecules* **1999**, *32*, 4439−4443.
(25) Flikkema, E.; Subbotin, A.; ten Brinke, G. Ring Comb Copolymer Brushes. *J. Chem. Phys.* **2000**, *113*, 7646−7651.
(26) Elli, S.; Ganazzoli, F.; Timoshenko, E. G.; Kuznetsov, Y. A.; Connolly, R. Size and Persistence Length of Molecular Bottle-Brushes by Monte Carlo Simulations. *J. Chem. Phys.* **2004**, *120*, 6257−6267.
(27) Connolly, R.; Bellesia, G.; Timoshenko, E. G.; Kuznetsov, Y. A.; Elli, S.; Ganazzoli, F. "Intrinsic" and "Topological" Stiffness in Branched Polymers. *Macromolecules* **2005**, *38*, 5288−5299.
(28) Yethiraj, A. A Monte Carlo Simulation Study of Branched Polymers. *J. Chem. Phys.* **2006**, *125*, 204901.
(29) Hsu, H.-P.; Paul, W.; Binder, K. Structure of Bottle-Brush Polymers in Solution: A Monte Carlo Test of Models for the Scattering Function. *J. Chem. Phys.* **2008**, *129*, 204904.
(30) Hsu, H.-P.; Paul, W.; Binder, K. Standard Definitions of Persistence Length Do Not Describe the Local "Intrinsic" Stiffness of Real Polymer Chains. *Macromolecules* **2010**, *43*, 3094−3102.
(31) Hsu, H.-P.; Paul, W.; Rathgeber, S.; Binder, K. Characteristic Length Scales and Radial Monomer Density Profiles of Molecular Bottle-Brushes: Simulation and Experiment. *Macromolecules* **2010**, *43*, 1592−1601.
(32) Hsu, H.-P.; Paul, W.; Binder, K. Polymer Chain Stiffness vs. Excluded Volume: A Monte Carlo Study of the Crossover towards the Worm-like Chain Model. *Europhys. Lett.* **2010**, *92*, 28003.
(33) Angelescu, D. G.; Linse, P. Monte Carlo Simulations of Multigraft Homopolymers in Good Solvent. *Macromolecules* **2013**, *47*, 415−426.
(34) Rouault, Y.; Borisov, O. V. Comb-Branched Polymers: Monte Carlo Simulation and Scaling. *Macromolecules* **1996**, *29*, 2605−2611.
(35) Shiokawa, K.; Itoh, K.; Nemoto, N. Simulations of the Shape of a Regularly Branched Polymer as a Model of a Polymacromonomer. *J. Chem. Phys.* **1999**, *111*, 8165−8173.
(36) Hsu, H.-P.; Paul, W.; Binder, K. Understanding the Multiple Length Scales Describing the Structure of Bottle-Brush Polymers by Monte Carlo Simulation Methods. *Macromol. Theory Simul.* **2011**, *20*, 510−525.
(37) Khalatur, P. G.; Shirvanyanz, D. G.; Starovoitova, N. Y.; Khokhlov, A. R. Conformational Properties and Dynamics of Molecular Bottle-Brushes: A cellular-automaton-based Simulation. *Macromol. Theory Simul.* **2000**, *9*, 141−155.
(38) Theodorakis, P. E.; Paul, W.; Binder, K. Microphase Separation in Bottlebrush Polymers under Poor-Solvent Conditions. *Europhys. Lett.* **2009**, *88*, 63002.
(39) Theodorakis, P. E.; Paul, W.; Binder, K. Pearl-Necklace Structures of Molecular Brushes with Rigid Backbone under Poor Solvent Conditions: A Simulation Study. *J. Chem. Phys.* **2010**, *133*, 104901.
(40) Theodorakis, P. E.; Hsu, H.-P.; Paul, W.; Binder, K. Computer Simulation of bottle-brush Polymers with Flexible Backbone: Good Solvent Versus Theta Solvent Conditions. *J. Chem. Phys.* **2011**, *135*, 164903.
(41) Carrillo, J.-M. Y.; Sheiko, S. S.; Dobrynin, A. V. Molecular Dynamics Simulations of Bottlebrush Macromolecules in Two Dimensional Polymeric Melts under Flow Conditions. *Soft Matter* **2011**, *7*, 2805.
(42) Maleki, H.; Theodorakis, P. E. Structure of Bottle-Brush Brushes under Good Solvent Conditions: A Molecular Dynamics Study. *J. Phys.: Condens. Matter* **2011**, *23*, 505104.
(43) Erukhimovich, I.; Theodorakis, P. E.; Paul, W.; Binder, K. Mesophase Formation in Two-Component Cylindrical Bottlebrush Polymers. *J. Chem. Phys.* **2011**, *134*, 054906.
(44) Theodorakis, P. E.; Fytas, N. G. Molecular Dynamics Simulations of Bottle-Brush Polymers with a Flexible Backbone under Theta and Good Solvent Conditions. *Am. J. Condens. Matter Phys.* **2012**, *2*, 101−108.
(45) Fytas, N. G.; Theodorakis, P. E. Molecular Dynamics Simulations of Single-Component Bottle-Brush Polymers with Flexible Backbones under Poor Solvent Conditions. *J. Phys.: Condens. Matter* **2013**, *25*, 285105.
(46) Zhang, Z.; Carrillo, J.-M. Y.; Ahn, S. K.; Wu, B.; Hong, K.; Smith, G. S.; Do, C. Atomistic Structure of Bottlebrush Polymers: Simulations and Neutron Scattering Studies. *Macromolecules* **2014**, *47*, 5808−5814.
(47) Cao, Z.; Carrillo, J.-M. Y.; Sheiko, S. S.; Dobrynin, A. V. Computer Simulations of Bottle Brushes: From Melts to Soft Networks. *Macromolecules* **2015**, *48*, 5006−5015.

DOI: 10.1021/acs.macromol.9b00363
Macromolecules 2019, 52, 4858−4874

(48) Cao, Z.; Daniel, W. F. M.; Vatankhah-Varnosfaderani, M.; Sheiko, S. S.; Dobrynin, A. V. Dynamics of Bottlebrush Networks. *Macromolecules* **2016**, *49*, 8009−8017.
(49) Chatterjee, D.; Vilgis, T. A. Scaling Laws of Bottle-Brush Polymers in Dilute Solutions. *Macromol. Theory Simul.* **2016**, *25*, 518−523.
(50) Liang, H.; Cao, Z.; Wang, Z.; Sheiko, S. S.; Dobrynin, A. V. Combs and Bottlebrushes in a Melt. *Macromolecules* **2017**, *50*, 3430−3437.
(51) Wessels, M. G.; Jayaraman, A. Molecular dynamics simulation study of linear, bottlebrush, and star-like amphiphilic block polymer assembly in solution. *Soft Matter* **2019**, *15*, 3987−3998.
(52) Dutta, S.; Wade, M. A.; Walsh, D. J.; Guironnet, D.; Rogers, S. A.; Sing, C. E. Dilute Solution Structure of Bottlebrush Polymers. *Soft Matter* **2019**, 2928.
(53) Feuz, L.; Leermakers, F. A. M.; Textor, M.; Borisov, O. Bending Rigidity and Induced Persistence Length of Molecular Bottle Brushes: A Self-Consistent-Field Theory. *Macromolecules* **2005**, *38*, 8891−8901.
(54) Dalsin, S. J.; Rions-Maehren, T. G.; Beam, M. D.; Bates, F. S.; Hillmyer, M. A.; Matsen, M. W. Bottlebrush Block Polymers: Quantitative Theory and Experiments. *ACS Nano* **2015**, *9*, 12233−12245.
(55) Lyubimov, I.; Wessels, M. G.; Jayaraman, A. Molecular Dynamics Simulation and PRISM Theory Study of Assembly in Solutions of Amphiphilic Bottlebrush Block Copolymers. *Macromolecules* **2018**, *51*, 7586−7599.
(56) Birshtein, T. M.; Borisov, O. V.; Zhulina, Y. B.; Khokhlov, A. R.; Yurasova, T. A. Conformations of Comb-like Macromolecules. *Polym. Sci. U.S.S.R.* **1987**, *29*, 1293−1300.
(57) Fredrickson, G. H. Surfactant-Induced Lyotropic Behavior of Flexible Polymer Solutions. *Macromolecules* **1993**, *26*, 2825−2831.
(58) Zhulina, E. B.; Vilgis, T. A. Scaling Theory of Planar Brushes Formed by Branched Polymers. *Macromolecules* **1995**, *28*, 1008−1015.
(59) Paturej, J.; Kreer, T. Hierarchical Excluded Volume Screening in Solutions of Bottlebrush Polymers. *Soft Matter* **2017**, *13*, 8534−8541.
(60) Wintermantel, M.; Schmidt, M.; Tsukahara, Y.; Kajiwara, K.; Kohjiya, S. Rodlike Combs. *Macromol. Rapid Commun.* **1994**, *15*, 279−284.
(61) Wintermantel, M.; Gerle, M.; Fischer, K.; Schmidt, M.; Wataoka, I.; Urakawa, H.; Kajiwara, K.; Tsukahara, Y. Molecular Bottlebrushes. *Macromolecules* **1996**, *29*, 978−983.
(62) Kawaguchi, S.; Akaike, K.; Zhang, Z.-M.; Matsumoto, H.; Ito, K. Water Soluble Bottlebrushes. *Polym. J.* **1998**, *30*, 1004−1007.
(63) Terao, K.; Takeo, Y.; Tazaki, M.; Nakamura, Y.; Norisuye, T. Polymacromonomer Consisting of Polystyrene. Light Scattering Characterization in Cyclohexane. *Polym. J.* **1999**, *31*, 193−198.
(64) Terao, K.; Nakamura, Y.; Norisuye, T. Solution Properties of Polymacromonomers Consisting of Polystyrene. 2. Chain Dimensions and Stiffness in Cyclohexane and Toluene. *Macromolecules* **1999**, *32*, 711−716.
(65) Terao, K.; Hokajo, T.; Nakamura, Y.; Norisuye, T. Solution Properties of Polymacromonomers Consisting of Polystyrene. 3. Viscosity Behavior in Cyclohexane and Toluene. *Macromolecules* **1999**, *32*, 3690−3694.
(66) Terao, K.; Hayashi, S.; Nakamura, Y.; Norisuye, T. Solution Properties of Polymacromonomers Consisting of Polystyrene. *Polym. Bull.* **2000**, *44*, 309−316.
(67) Hokajo, T.; Terao, K.; Nakamura, Y.; Norisuye, T. Solution Properties of Polymacromonomers Consisting of Polystyrene V. Effect of Side Chain Length on Chain Stiffness. *Polym. J.* **2001**, *33*, 481−485.
(68) Hokajo, T.; Hanaoka, Y.; Nakamura, Y.; Norisuye, T. Translational Diffusion Coefficient of Polystyrene Polymacromonomers. Dependence on Side-Chain Length. *Polym. J.* **2005**, *37*, 529−534.
(69) Amitani, K.; Terao, K.; Nakamura, Y.; Norisuye, T. Small-Angle X-Ray Scattering from Polystyrene Polymacromonomers in Cyclohexane. *Polym. J.* **2005**, *37*, 324−331.
(70) Inoue, K.; Yamamoto, S.; Nakamura, Y. Dilute Solution Properties of a Polymacromonomer Consisting of a Polystyrene Main Chain with Polyisoprene Side Chains. Relation of Molecular Parameters to Polymer Segment Interactions. *Macromolecules* **2013**, *46*, 8664−8670.
(71) Kikuchi, M.; Mihara, T.; Jinbo, Y.; Izumi, Y.; Nagai, K.; Kawaguchi, S. Characterization of Rodlike Poly(N-Hexyl Isocyanate) Macromonomers and their Polymacromonomers by Light Scattering, SAXS, Intrinsic Viscosity, and Scanning Force Microscopy. *Polym. J.* **2007**, *39*, 330−341.
(72) Kikuchi, M.; Lien, L. T. N.; Narumi, A.; Jinbo, Y.; Izumi, Y.; Nagai, K.; Kawaguchi, S. Conformational Properties of Cylindrical Rod Brushes Consisting of a Polystyrene Main Chain and Poly(N-Hexyl Isocyanate) Side Chains. *Macromolecules* **2008**, *41*, 6564−6572.
(73) Saito, Y.; Lien, L. T. N.; Jinbo, Y.; Kumaki, J.; Narumi, A.; Kawaguchi, S. Influence of the Primary Structure of the Main Chain on Backbone Stiffness of Cylindrical Rod Brushes. *Polym. J.* **2013**, *45*, 193−201.
(74) Kikuchi, M.; Nakano, R.; Jinbo, Y.; Saito, Y.; Ohno, S.; Togashi, D.; Enomoto, K.; Narumi, A.; Haba, O.; Kawaguchi, S. Graft Density Dependence of Main Chain Stiffness in Molecular Rod Brushes. *Macromolecules* **2015**, *48*, 5878−5886.
(75) Kikuchi, M.; Takahara, A.; Kawaguchi, S. Dimensional Characterizations from Rod Stars to Brushes of Polymers with a Low Degree of Polymerization. *Macromolecules* **2016**, *50*, 324−331.
(76) Nakamura, Y.; Norisuye, T. Brush-like polymers. In *Soft Matter Characterization*; Springer Netherlands: Dordrecht, 2008; pp 235−286.
(77) Gerle, M.; Fischer, K.; Roos, S.; Müller, A. H. E.; Schmidt, M.; Sheiko, S. S.; Prokhorova, S.; Möller, M. Main Chain Conformation and Anomalous Elution Behavior of Cylindrical Brushes as Revealed by GPC/MALLS, Light Scattering, and SFM. *Macromolecules* **1999**, *32*, 2629−2637.
(78) Rathgeber, S.; Pakula, T.; Wilk, A.; Matyjaszewski, K.; Beers, K. L. On the Shape of Bottle-Brush Macromolecules: Systematic Variation of Architectural Parameters. *J. Chem. Phys.* **2005**, *122*, 124904.
(79) Zhao, Y.; Jamieson, A. M.; Olson, B. G.; Yao, N.; Dong, S.; Nazarenko, S.; Hu, X.; Lal, J. Conformation of Comb-like Liquid Crystal Polymers in Isotropic Solution Probed by Small-Angle Neutron Scattering. *J. Polym. Sci., Part B: Polym. Phys.* **2006**, *44*, 2412−2424.
(80) Gunari, N.; Schmidt, M.; Janshoff, A. Persistence Length of Cylindrical Brush Molecules Measured by Atomic Force Microscopy. *Macromolecules* **2006**, *39*, 2219−2224.
(81) Kremer, K.; Grest, G. S. Dynamics of Entangled Linear Polymer melts: A molecular-dynamics Simulation. *J. Chem. Phys.* **1990**, *92*, 5057−5086.
(82) Weeks, J. D.; Chandler, D.; Andersen, H. C. Role of Repulsive Forces in Determining the Equilibrium Structure of Simple Liquids. *J. Chem. Phys.* **1971**, *54*, 5237−5247.
(83) Ermak, D. L.; McCammon, J. A. Brownian Dynamics with Hydrodynamic Interactions. *J. Chem. Phys.* **1978**, *69*, 1352−1360.
(84) Dünweg, B.; Reith, D.; Steinhauser, M.; Kremer, K. Corrections to Scaling in the Hydrodynamic Properties of Dilute Polymer Solutions. *J. Chem. Phys.* **2002**, *117*, 914−924.
(85) Rotne, J.; Prager, S. Variational Treatment of Hydrodynamic Interaction in Polymers. *J. Chem. Phys.* **1969**, *50*, 4831−4837.
(86) Yamakawa, H. Transport Properties of Polymer Chains in Dilute Solution: Hydrodynamic Interaction. *J. Chem. Phys.* **1970**, *53*, 436−443.
(87) Carrasco, B.; de la Torre, J. G. Hydrodynamic Properties of Rigid Particles: Comparison of Different Modeling and Computational Procedures. *Biophys. J.* **1999**, *76*, 3044−3057.
(88) de la Torre, J. G.; Lopez Martinez, M. C.; Tirado, M. M. Monte Carlo Study of Hydrodynamic Properties of Flexible Linear Chains:

DOI: 10.1021/acs.macromol.9b00363
Macromolecules 2019, 52, 4858−4874

Analysis of Several Approximate Methods. *Macromolecules* **1984**, *17*, 2715−2722.
(89) Tsuda, K. Intrinsic Viscosity of Rigid Complex Molecules. *Rheol. Acta* **1970**, *9*, 509−516.
(90) Tsuda, K. Hydrodynamic Properties of Rigid Complex Molecules. *Polym. J.* **1970**, *1*, 616−631.
(91) Benoit, H.; Doty, P. Light Scattering from Non-gaussian Chains. *J. Phys. Chem.* **1953**, *57*, 958−963.
(92) Yamakawa, H.; Yoshizaki, T. *Helical Wormlike Chains in Polymer Solutions*, 2nd ed.; Springer-Verlag: Berlin Heidelberg, 2016.
(93) Konishi, T.; Yoshizaki, T.; Saito, T.; Einaga, Y.; Yamakawa, H. Mean-Square Radius of Gyration of Oligo- and Polystyrenes in Dilute Solutions. *Macromolecules* **1990**, *23*, 290−297.
(94) Forsman, W. C. In *Polymers in Solution*; Statistics and dynamics of polymer molecules in solution, Forsman, W. C., Ed.; Springer Science+Business Media N.Y., 1986; pp 1−110.
(95) Yamakawa, H.; Fujii, M. Translational Friction Coefficient of Wormlike Chains. *Macromolecules* **1973**, *6*, 407−415.
(96) Norisuye, T.; Motowoka, M.; Fujita, H. Wormlike Chains near the Rod Limit: Translational Friction Coefficient. *Macromolecules* **1979**, *12*, 320−323.
(97) Yoshizaki, T.; Nitta, I.; Yamakawa, H. Transport Coefficients of Helical Wormlike Chains. 4. Intrinsic Viscosity of the Touched-Bead Model. *Macromolecules* **1988**, *21*, 165−171.
(98) Paturej, J.; Sheiko, S. S.; Panyukov, S.; Rubinstein, M. Molecular Structure of Bottlebrush Polymers in Melts. *Sci. Adv.* **2016**, *2*, No. e1601478.
(99) Pedersen, J. S.; Schurtenberger, P. Scattering Functions of Semiflexible Polymers with and without Excluded Volume Effects. *Macromolecules* **1996**, *29*, 7602−7612.
(100) Fischer, K.; Schmidt, M. Solvent-Induced Length Variation of Cylindrical Brushes. *Macromol. Rapid Commun.* **2001**, *22*, 787−791.
(101) Hsu, H.-P.; Paul, W.; Binder, K. Estimation of Persistence Lengths of Semiflexible Polymers: Insight from Simulations. *Polym. Sci., Ser. C* **2013**, *55*, 39−59.
(102) Gubarev, A.; Carrillo, J.-M. Y.; Dobrynin, A. V. Scale-Dependent Electrostatic Stiffening in Biopolymers. *Macromolecules* **2009**, *42*, 5851−5860.
(103) Subbotin, A.; Saariaho, M.; Ikkala, O.; ten Brinke, G. Elasticity of Comb Copolymer Cylindrical Brushes. *Macromolecules* **2000**, *33*, 3447−3452.
(104) Nakamura, Y.; Norisuye, T. Backbone Stiffness of Comb-Branched Polymers. *Polym. J.* **2001**, *33*, 874−878.
(105) Onsager, L. The Effects of Shape on the Interaction of Colloidal Particles. *Ann. N. Y. Acad. Sci.* **1949**, *51*, 627−659.
(106) Chen, Z. Y.; Noolandi, J. Renormalization-Group Scaling Theory for Flexible and Wormlike Polymer Chains. *J. Chem. Phys.* **1992**, *96*, 1540−1548.
(107) Tree, D. R.; Muralidhar, A.; Doyle, P. S.; Dorfman, K. D. Is DNA a Good Model Polymer? *Macromolecules* **2013**, *46*, 8369−8382.
(108) Gu, W.; Huh, J.; Hong, S. W.; Sveinbjornsson, B. R.; Park, C.; Grubbs, R. H.; Russell, T. P. Self-Assembly of Symmetric Brush Diblock Copolymers. *ACS Nano* **2013**, *7*, 2551−2558.
(109) Verduzco, R.; Li, X.; Pesek, S. L.; Stein, G. E. Structure, Function, Self-Assembly, and Applications of Bottlebrush Copolymers. *Chem. Soc. Rev.* **2015**, *44*, 2405−2420.
(110) Lin, T.-P.; Chang, A. B.; Luo, S.-X.; Chen, H.-Y.; Lee, B.; Grubbs, R. H. Effects of Grafting Density on Block Polymer Self-Assembly: From Linear to Bottlebrush. *ACS Nano* **2017**, *11*, 11632−11641.
(111) Sunday, D. F.; Chang, A. B.; Liman, C. D.; Gann, E.; Delongchamp, D. M.; Thomsen, L.; Matsen, M. W.; Grubbs, R. H.; Soles, C. L. Self-Assembly of ABC Bottlebrush Triblock Terpolymers with Evidence for Looped Backbone Conformations. *Macromolecules* **2018**, *51*, 7178−7185.
(112) Radzinski, S. C.; Foster, J. C.; Scannelli, S. J.; Weaver, J. R.; Arrington, K. J.; Matson, J. B. Tapered Bottlebrush Polymers: Cone-Shaped Nanostructures by Sequential Addition of Macromonomers. *ACS Macro Lett.* **2017**, *6*, 1175−1179.
(113) Walsh, D. J.; Guironnet, D. Macromolecules with Programmable Shape, Size, and Chemistry. *Proc. Natl. Acad. Sci. U. S. A.* **2019**, *116*, 1538.

DOI: 10.1021/acs.macromol.9b00363
Macromolecules 2019, 52, 4858−4874